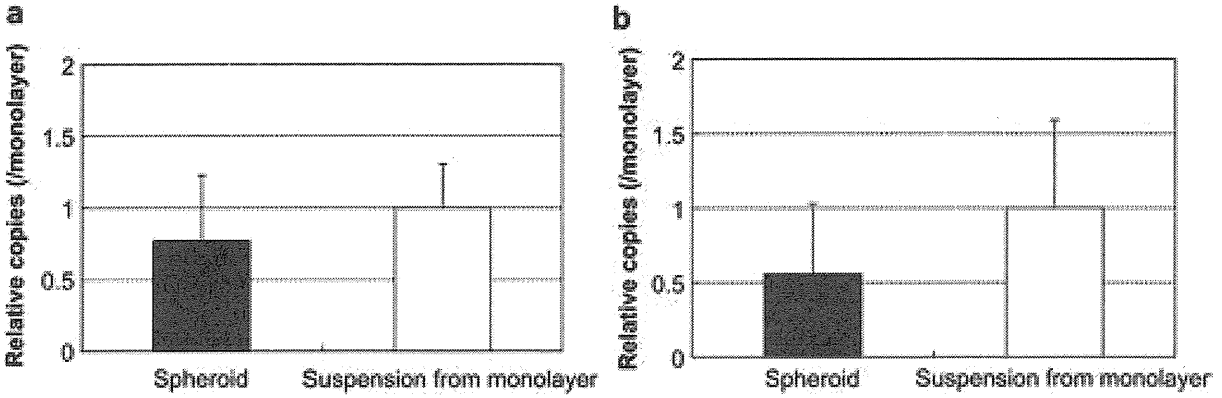

Fig. 4. Evaluation of the cell number of transplanted hepatocytes and copy number of transfected luciferase pDNA in the host tissue. After 24 h of transfection with luciferase-expressing pDNA, hepatocyte spheroids and a single-cell suspension from a monolayer culture were transplanted into the subcutaneous tissue of mouse forelimbs. At 24 h after transplantation, total DNA was extracted from the transplantation site for the following analyses: (a) The number of transplanted hepatocytes was measured using quantitative real-time PCR (qRT-PCR) analysis of the SRY gene on the Y chromosome, (b) copy number of luciferase pDNA was measured using qRT-PCR. The data are presented as the mean ± standard error of the mean (s.e.m.) ($N = 7$).

albumin. As shown in Fig. 5, the hepatocyte spheroids showed significantly higher albumin expression in the host tissue compared with that in hepatocytes from the monolayer culture. This result of preserved albumin secretion in spheroids is consistent with the previous *in vitro* study results showing sustained albumin secretion in the culture medium from hepatocyte spheroids [7,13], indicating that spheroid formation essentially contributes to the maintenance of innate functions, such as albumin secretion of hepatocytes in both *in vitro* culture and *in vivo* transplantation.

To further analyze cell behavior in the host tissue, we performed imaging of the transplanted cells in the tissue using intravital confocal microscopy [26]. Hepatocytes from transgenic rats stably expressing enhanced green fluorescent protein (EGFP) were transplanted into the earlobes of mice without EGFP expression in the form of either spheroids or a single-cell suspension, followed by *in vivo* imaging 24 h after transplantation. Fig. 6a, b shows typical images exhibiting the distribution of transplanted EGFP-positive cells. Of interest, in the spheroid-transplanted mice, the EGFP fluorescence was obviously aligned with blood vessels. The proximity of spheroids to the vessels was confirmed in high-resolution images with co-staining of the vessels by Evans blue (Fig. 6c). In contrast, the distribution of hepatocytes from monolayer cultures showed no specific pattern (Fig. 6b.) Although the detailed mechanism of the difference in cell distribution in the host tissue is yet to be clarified, the localized alignment in the vicinity of blood vessels is definitely an advantage of the spheroid systems for providing a favorable microenvironment to preserve cell activity.

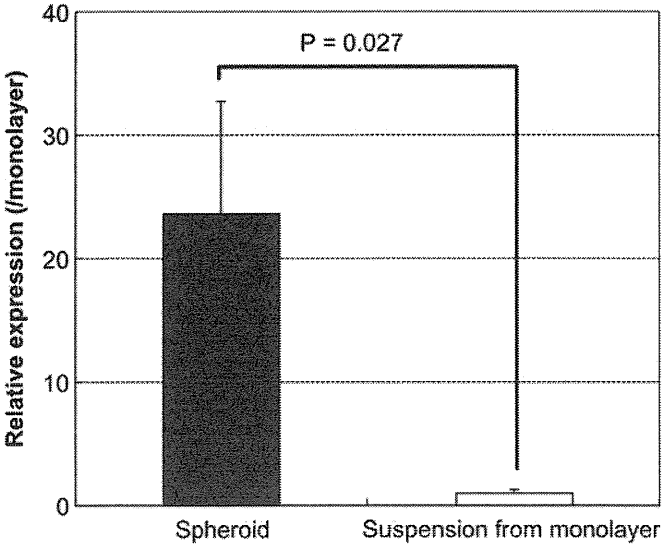

Fig. 5. Albumin expression from transplanted hepatocytes in the host tissue. After 24 h of transfection with luciferase-expressing pDNA, hepatocyte spheroids and single-cell suspensions from monolayer cultures were transplanted into the subcutaneous tissue of mouse forelimbs. At 24 h after transplantation, mRNA expression levels of rat albumin in the forelimb were measured using quantitative real-time PCR (qRT-PCR). The data are presented as the mean ± standard error of the mean (s.e.m.) ($N = 8$). Statistical significance was assessed by 2-tailed Student's *t*-test.

3.3. Hematopoiesis after transplantation of erythropoietin-introduced hepatocyte spheroids

To investigate the feasibility of spheroid transplantation for therapeutic purposes, hepatocyte spheroids receiving transfection with erythropoietin-expressing pDNA were transplanted into the subcutaneous tissue of mice, followed by the evaluation of the hematopoietic effect induced by erythropoietin [31]. A single-cell suspension of hepatocytes from a monolayer culture was used as the control. After the transplantation of erythropoietin-expressing hepatocyte spheroids, the hematocrit and hemoglobin levels showed significant increases in host mice on days 22 and 28 (Fig. 7). In contrast, hepatocytes from monolayer cultures induced only marginal increases in hematocrit and hemoglobin levels, suggesting that spheroid transplantation was more beneficial than transplantation of cells from monolayer cultures to obtain therapeutic efficacy by transgene expression.

4. Discussion

In this study, we demonstrated an effective cell transplantation for therapeutic purpose by combining two of our original technologies, non-viral gene transfection vector, and micropatterned spheroid culture plates. Using the micropatterned plates, the size of spheroids was controlled in a narrow range around 100 μm to maintain functionality and survival of the cells in spheroids. Indeed, in the previous reports, optimal size of hepatocyte spheroids to obtain maximal secretion of albumin in cultured condition was determined to be 100 μm, while spheroids with the size of more than several hundred μm resulted in the necrosis of inner core [32–34]. By using micropatterned culture plates, we succeeded in the preparation of spheroids with uniform size of 100 μm, whereas

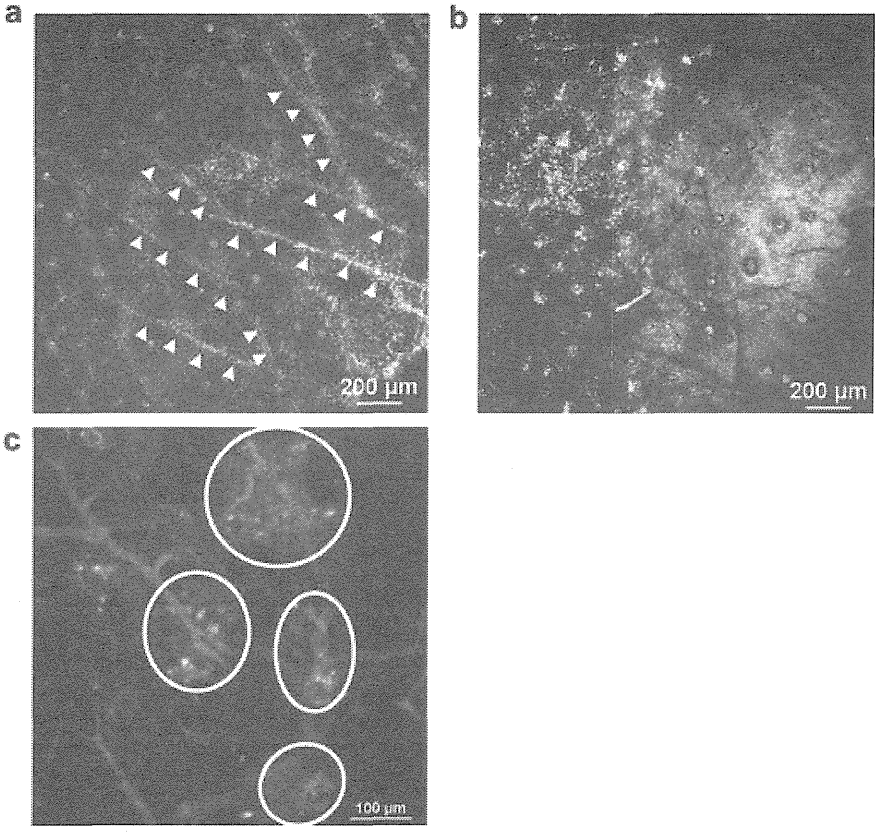

Fig. 6. Intravital microscopic imaging of transplanted hepatocytes in the host tissue. Hepatocytes stably expressing enhanced green fluorescence protein (EGFP, green) were used to track the transplanted cells. After 24 h of transfection with luciferase-expressing pDNA, the hepatocytes were subcutaneously transplanted into mouse earlobes. At 24 h after transplantation, earlobes were observed using an intravital confocal laser scanning microscope. (a, b) Broad field images after the transplantation of (a) hepatocyte spheroids and (b) single-cell suspension from a monolayer culture. Arrowheads indicate alignment of transplanted cells along blood vessels. (c) High-resolution images with co-staining of blood vessels by intravenous injection of Evans blue (red) after the transplantation of hepatocyte spheroids. Circles indicate association of transplanted cells with the blood vessels. (For interpretation of the references to color in this figure legend, the reader is referred to the web version of this article.)

precise control of spheroid size was difficult in other commonly used methods, such as those using spinner flasks, and non-adhesive culture plates, and hanging-drop methods [10,35–37]. It should be emphasized that the uniform size of spheroids with relatively small diameter of 100 μm makes it possible to transplant the spheroids by commonly used injection needle. The ease of spheroid preparation even in a large-scale using the micropatterned plates (maximum of 2,500 spheroids per cm^2 culture plate) and the practicability of

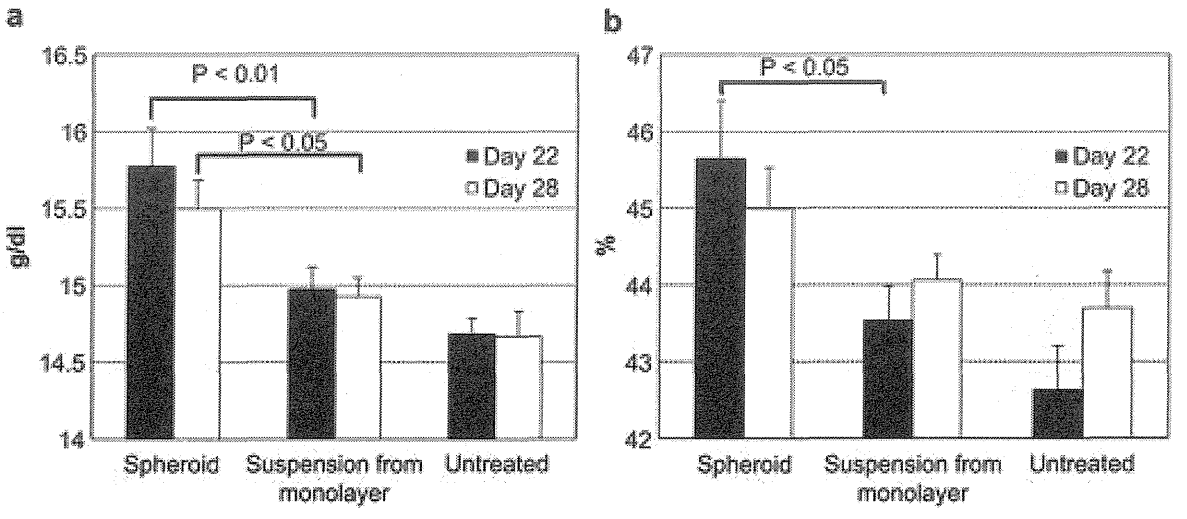

Fig. 7. Hematopoiesis after transplantation of erythropoietin-introduced hepatocytes. Hepatocytes in spheroid and monolayer cultures were transfected with erythropoietin-expressing pDNA. At 24 h of transfection, these spheroids and single-cell suspensions from monolayer cultures were subcutaneously transplanted into mouse abdomens. At 22 and 28 days after transplantation, hemoglobin (a) and hematocrit (b) levels were measured from blood samples. The data are presented as the mean ± standard error of the mean (s.e.m.). ($N = 12$ for spheroid and monolayer groups, and $N = 6$ for untreated controls). Statistical significance was assessed by 2-tailed Student's t-test.

transplantation by injection needles with maintaining the spheroid structure is particularly useful for future clinical application.

The other aspect of this system is the genetic modification of the spheroids by gene introduction using polyplex nanomicelles. The transgene expression from the spheroids exceeded 10 folds compared with the hepatocytes from monolayer cultures in host mice after transplantation (Fig. 2). To confirm the potential of this system for therapeutic application, we used erythropoietin-expressing pDNA for genetic modification. Erythropoietin is a systemically-secreted hormone produced by kidney peritubular interstitial cells in adult mammals, stimulating the production of red blood cells [31], Recombinant erythropoietin is clinically used as a hematopoietic factor [38]; however, the short duration of action of recombinant erythropoietin may necessitate multiple doses to obtain a continuous effect on hematopoiesis. In this study, a single transplantation procedure for erythropoietin-introduced hepatocyte spheroids was demonstrated to induce a hematopoietic effect in host mice for more than a month. The effect was significantly higher than that produced by cell transplantation from a monolayer culture (Fig. 6). Thus, it was revealed that the sustained manner of transgene expression from the spheroids was beneficial to obtain a therapeutic effect by secretion of bioactive factors such as erythropoietin from the transplanted cells into host mice.

It is interesting that in the *in vitro* study, transgene expression was comparable between the spheroid and monolayer culture groups (Fig. 3). In addition, the total cell number surviving in the host tissue after transplantation was comparable between these two groups (Fig. 4). We assumed that the increased transgene expression from the spheroids was attributed to the enhanced functionality of individual cells in the spheroids. Indeed, albumin expression as a marker for the innate function of transplanted hepatocytes significantly increased in spheroid systems (Fig. 5). For further investigation of the mechanism, we performed intravital imaging of the transplanted cells in the host tissue. As shown in Fig. 6, the cells transplanted as spheroid form had a tendency to locate in the vicinity of blood vessels, while the cells from the monolayer culture showed no specific distribution pattern. Thus, it is likely that the transplantation in spheroid form affected the subsequent cell behavior in the host tissue to accumulate near the blood vessels, resulting in prolonged secretion of erythropoietin. Regarding the unique image shown in Fig. 6a, c that the transplanted hepatocytes accumulated to the vicinity of the vessels, it is still unclear whether these cells migrate as the group of spheroids or individual cells from the disintegrated spheroids direct to the vessels. Although the detailed mechanism is yet to be clarified, the accumulation of transplanted hepatocytes into the vicinity of the vasculature is apparently beneficial to exert their proper functionality. Presumably, the molecule regulating cell adhesion such as CXCR4, which were reported to be upregulated in MSC spheroids compared with that in cells in monolayer culture [39], may play a crucial role to regulate the cell-to-cell interaction with the host cells and the extracellular matrix in the host tissue.

5. Conclusion

We established an effective platform for cell transplantation by a combined use of micropatterned spheroid culture on thermosensitive plates with a non-viral gene introduction system of polyplex nanomicelle. The hepatocyte spheroids could be recovered simply by lowering temperature with maintaining the spheroid structure after gene introduction. The spheroids were injectable directly into host animals by needles, where the transgene expression as well as innate functionality of hepatocytes represented by secretion of albumin was effectively preserved in host tissue for more than a month. The transplantation of hepatocyte spheroids receiving erythropoietin-expressing pDNA provided sustained therapeutic effect of enhanced hematopoiesis in host animals, demonstrating the high potential of this system for therapeutic cell transplantation.

Acknowledgments

This work was financially supported in part by Grants-in-Aid for Scientific Research form the Japanese Ministry of Education, Culture, Sports, Science and Technology, Japan (MEXT) (K. I.), Global COE Program "Medical System Innovation through Multidisciplinary Integration" from MEXT, Japan, and Funding Program for World-Leading Innovative R&D on Science and Technology (FIRST Program) from the Japan Society for the Promotion of Science (JSPS). We thank Satomi Ogura, Asuka Miyoshi, Tomoko Tamamoto and Katsue Morii (The University of Tokyo) for technical assistance.

Appendix A. Supplementary data

Supplementary data related to this article can be found at http://dx.doi.org/10.1016/j.biomaterials.2013.12.012

References

[1] Lavasani M, Robinson AR, Lu A, Song M, Feduska JM, Ahani B, et al. Muscle-derived stem/progenitor cell dysfunction limits healthspan and lifespan in a murine progeria model. Nat Commun 2012;3:608.
[2] Haider H, Mustafa A, Feng Y, Ashraf M. Genetic modification of stem cells for improved therapy of the infarcted myocardium. Mol Pharmacol 2011;8:1446–57.
[3] Meyerrose T, Olson S, Pontow S, Kalomoiris S, Jung Y, Annett G, et al. Mesenchymal stem cells for the sustained in vivo delivery of bioactive factors. Adv Drug Deliv Rev 2010;62:1167–74.
[4] Porada CD, Almeida-Porada G. Mesenchymal stem cells as therapeutics and vehicles for gene and drug delivery. Adv Drug Deliv Rev 2010;62:1156–66.
[5] Sheyn D, Mizrahi O, Benjamin S, Gazit Z, Pelled G, Gazit D. Genetically modified cells in regenerative medicine and tissue engineering. Adv Drug Deliv Rev 2010;62:683–98.
[6] Robey TE, Saiget MK, Reinecke H, Murry CE. Systems approaches to preventing transplanted cell death in cardiac repair. J Mol Cell Cardiol 2008;45:567–81.
[7] Otsuka H, Hirano A, Nagasaki Y, Okano T, Horiike Y, Kataoka K. Two-dimensional multiarray formation of hepatocyte spheroids on a microfabricated PEG-brush surface. Chembiochem 2004;5:850–5.
[8] Landry J, Bernier D, Ouellet C, Goyette R, Marceau N. Spheroidal aggregate culture of rat liver cells: histotypic reorganization, biomatrix deposition, and maintenance of functional activities. J Cell Biol 1985;101:914–23.
[9] Yuasa C, Tomita Y, Shono M, Ishimura K, Ichihara A. Importance of cell aggregation for expression of liver functions and regeneration demonstrated with primary cultured hepatocytes. J Cell Physiol 1993;156:522–30.
[10] Bartosh TJ, Ylostalo JH, Mohammadipoor A, Bazhanov N, Coble K, Claypool K, et al. Aggregation of human mesenchymal stromal cells (MSCs) into 3D spheroids enhances their antiinflammatory properties. Proc Natl Acad Sci U S A 2010;107:13724–9.
[11] Frith JE, Thomson B, Genever PG. Dynamic three-dimensional culture methods enhance mesenchymal stem cell properties and increase therapeutic potential. Tissue Eng Part C Methods 2010;16:735–49.
[12] Wang W, Itaka K, Ohba S, Nishiyama N, Chung UI, Yamasaki Y, et al. 3D spheroid culture system on micropatterned substrates for improved differentiation efficiency of multipotent mesenchymal stem cells. Biomaterials 2009;30:2705–15.
[13] Endo T, Itaka K, Shioyama M, Uchida S, Kataoka K. Gene transfection to spheroid culture system on micropatterned culture plate by polyplex nanomicelle: a novel platform of genetically-modified cell transplantation. Drug Deliv Trans Res 2012;2:398–405.
[14] Kataoka K, Harada A, Nagasaki Y. Block copolymer micelles for drug delivery: design, characterization and biological significance. Adv Drug Deliv Rev 2001;47:113–31.
[15] Itaka K, Kataoka K. Recent development of nonviral gene delivery systems with virus-like structures and mechanisms. Eur J Pharm Biopharm 2009;71:475–83.
[16] Itaka K, Kataoka K. Progress and prospects of polyplex nanomicelles for plasmid DNA delivery. Curr Gene Ther 2011;11:457–65.
[17] Kanayama N, Fukushima S, Nishiyama N, Itaka K, Jang WD, Miyata K, et al. A PEG-based biocompatible block catiomer with high buffering capacity for the construction of polyplex micelles showing efficient gene transfer toward primary cells. ChemMedChem 2006;1:439–44.

[18] Miyata K, Oba M, Nakanishi M, Fukushima S, Yamasaki Y, Koyama H, et al. Polyplexes from poly(aspartamide) bearing 1,2-diaminoethane side chains induce pH-selective, endosomal membrane destabilization with amplified transfection and negligible cytotoxicity. J Am Chem Soc 2008;130:16287–94.
[19] Itaka K, Ishii T, Hasegawa Y, Kataoka K. Biodegradable polyamino acid-based polycations as safe and effective gene carrier minimizing cumulative toxicity. Biomaterials 2010;31:3707–14.
[20] Howard RB, Christensen AK, Gibbs FA, Pesch LA. The enzymatic preparation of isolated intact parenchymal cells from rat liver. J Cell Biol 1967;35:675–84.
[21] Berry MN, Friend DS. High-yield preparation of isolated rat liver parenchymal cells: a biochemical and fine structural study. J Cell Biol 1969;43:506–20.
[22] Tateno C, Yoshizato K. Long-term cultivation of adult rat hepatocytes that undergo multiple cell divisions and express normal parenchymal phenotypes. Am J Pathol 1996;148:383–92.
[23] Uchida S, Itaka K, Chen Q, Osada K, Ishii T, Shibata MA, et al. PEGylated polyplex with optimized PEG shielding enhances gene introduction in lungs by minimizing inflammatory responses. Mol Ther 2012;20:1196–203.
[24] Chen Q, Osada K, Ishii T, Oba M, Uchida S, Tockary TA, et al. Homo-catiomer integration into PEGylated polyplex micelle from block-catiomer for systemic anti-angiogenic gene therapy for fibrotic pancreatic tumors. Biomaterials 2012;33:4722–30.
[25] Wurdinger T, Badr C, Pike L, de Kleine R, Weissleder R, Breakefield XO, et al. A secreted luciferase for ex vivo monitoring of in vivo processes. Nat Methods 2008;5:171–3.
[26] Matsumoto Y, Nomoto T, Cabral H, Watanabe S, Christie RJ, Miyata K, et al. Direct and instantaneous observation of intravenously injected substances using intravital confocal micro-videography. Biomed Opt Express 2010;1:1209–16.
[27] Yang J, Yamato M, Kohno C, Nishimoto A, Sekine H, Fukai F, et al. Cell sheet engineering: recreating tissues without biodegradable scaffolds. Biomaterials 2005;26:6415–22.
[28] Ohashi K, Yokoyama T, Yamato M, Kuge H, Kanehiro H, Tsutsumi M, et al. Engineering functional two- and three-dimensional liver systems in vivo using hepatic tissue sheets. Nat Med 2007;13:880–5.
[29] Nishida K, Yamato M, Hayashida Y, Watanabe K, Yamamoto K, Adachi E, et al. Corneal reconstruction with tissue-engineered cell sheets composed of autologous oral mucosal epithelium. N Engl J Med 2004;351:1187–96.
[30] Pelzer M, Larsen M, Friedrich PF, Aleff RA, Bishop AT. Repopulation of vascularized bone allotransplants with recipient-derived cells: detection by laser capture microdissection and real-time PCR. J Orthop Res 2009;27:1514–20.
[31] Kreiss P, Bettan M, Crouzet J, Scherman D. Erythropoietin secretion and physiological effect in mouse after intramuscular plasmid DNA electrotransfer. J Gene Med 1999;1:245–50.
[32] Groebe K, Mueller-Klieser W. On the relation between size of necrosis and diameter of tumor spheroids. Int J Radiat Oncol Biol Phys 1996;34:395–401.
[33] Glicklis R, Merchuk JC, Cohen S. Modeling mass transfer in hepatocyte spheroids via cell viability, spheroid size, and hepatocellular functions. Biotechnol Bioeng 2004;86:672–80.
[34] Sakai Y, Nakazawa K. Technique for the control of spheroid diameter using microfabricated chips. Acta Biomater 2007;3:1033–40.
[35] Bhang SH, Cho SW, La WG, Lee TJ, Yang HS, Sun AY, et al. Angiogenesis in ischemic tissue produced by spheroid grafting of human adipose-derived stromal cells. Biomaterials 2011;32:2734–47.
[36] Yap KK, Dingle AM, Palmer JA, Dhillon RS, Lokmic Z, Penington AJ, et al. Enhanced liver progenitor cell survival and differentiation in vivo by spheroid implantation in a vascularized tissue engineering chamber. Biomaterials 2013;34:3992–4001.
[37] Lee EJ, Park SJ, Kang SK, Kim GH, Kang HJ, Lee SW, et al. Spherical bullet formation via E-cadherin promotes therapeutic potency of mesenchymal stem cells derived from human umbilical cord blood for myocardial infarction. Mol Ther 2012;20:1424–33.
[38] Macdougall IC, Tucker B, Thompson J, Tomson CR, Baker LR, Raine AE. A randomized controlled study of iron supplementation in patients treated with erythropoietin. Kidney Int 1996;50:1694–9.
[39] Potapova IA, Brink PR, Cohen IS, Doronin SV. Culturing of human mesenchymal stem cells as three-dimensional aggregates induces functional expression of CXCR4 that regulates adhesion to endothelial cells. J Biol Chem 2008;283:13100–7.

siRNA Conjugates

DOI: 10.1002/anie.201300178

Acidic pH-Responsive siRNA Conjugate for Reversible Carrier Stability and Accelerated Endosomal Escape with Reduced IFNα-Associated Immune Response**

Hiroyasu Takemoto, Kanjiro Miyata, Shota Hattori, Takehiko Ishii, Tomoya Suma, Satoshi Uchida, Nobuhiro Nishiyama, and Kazunori Kataoka**

Small interfering RNA (siRNA) has garnered much interest as a potential drug because of its strong gene-silencing activity.[1] Toward the success in siRNA therapeutics, many strategies have been developed for efficient siRNA delivery into the cytosol of target cells.[2] Among them, siRNA conjugates have arisen as one of the promising strategies in siRNA delivery, as siRNA can be readily conjugated to a functional molecule to acquire the ability of "programmed transfer" to the target sites.[3] Indeed, several ligand molecules, such as lactose and RGD peptide, were conjugated with siRNA for site- (or cell)-specific delivery.[3] Furthermore, multimolecular siRNA conjugates enable stable polyion complex (PIC) formation because of the increased electrostatic interactions with polycations, leading to facilitated cellular uptake through charge neutralization of siRNA and also protection of siRNA from enzymatic degradations.[4] However, those siRNA conjugates potentially stimulate immune responses through the activation of toll-like receptor 3 and/or protein kinase R,[4,5] and thus they are desired to disintegrate into monomeric siRNAs (mono-siRNAs) in the cell for reduced immune responses.[4] Meanwhile, considering that macromolecular drugs, including siRNA and its conjugates, would be taken up by cells through endocytosis and then delivered to the late endosome toward lysosomal degradation, siRNA needs to escape from the endosome into the cytosol for efficient gene silencing.[6] Therefore, design of a smart siRNA conjugate for programmed endosomal escape and release of mono-siRNA is a great challenge for successful siRNA delivery.

Herein, we developed a smart siRNA conjugate to fulfill the multifunctionality desired for enhanced siRNA delivery with reduced immunogenicity; that is, reversible PIC stability, endosomal escapability, and mono-siRNA releasability, based on a single chemical process. It is known that maleic acid amide (MAA) is relatively stable at extracellular neutral pH, while rapidly hydrolyzed at endosomal acidic pH.[7] Thus, we utilized this MAA chemistry as an acid-labile anionic moiety for linking siRNA to an endosome-disrupting polycation and concurrently converting the cationic sites into a biologically inert anionic derivative.[8] In design, the MAA-based conjugate is expected to improve the PIC stability through increased electrostatic interaction, while degrading the MAA moieties in the endosome for triggering three actions: 1) complex destabilization through unbalanced charges within PICs; 2) endosome disruption with the regenerated parent polycation; and 3) mono-siRNA release by MAA cleavage (Figure 1a). Figure 1b shows the chemical structure of siRNA-releasable/endosome-disrupting conjugate (REC), in which several siRNA molecules are grafted into the endosome-disrupting polymer side chains by the MAA linkage. The parent polycation is a polyaspartamide derivative with two repeating units of aminoethylene in each side chain (termed PAsp(DET)), which destabilizes the endosomal membrane integrity with the cationic diprotonated side chains to accelerate endosomal escape of the payload.[9]

A precursor polyanion was synthesized from PAsp(DET) to have a dibenzyl cyclooctyne (DBCO) group by MAA linkage as a conjugation site for siRNA. Then, an azide-modified siRNA (azide-siRNA) was reacted with the DBCO group in the polyanion side chains. Notably, the size exclusion chromatography (Supporting Information, Figure S5) confirmed that more than 95% of azide-siRNAs were conjugated to the polymer backbone utilizing a freeze–thaw treatment for the generation of a highly concentrated reactant phase.[10] This successful conjugation at the quite high rate allows the use of the obtained conjugate without further purification. As a result, about 30% of DBCO groups in the polymer side chains reacted with azide-siRNA; that is, about 5 siRNAs contained in the conjugate (Figure 1b). To investigate the

[*] H. Takemoto, Dr. K. Kataoka
Department of Materials Engineering, The University of Tokyo
Hongo 7-3-1, Bunkyo-ku, Tokyo 113-8656 (Japan)
E-mail: kataoka@bmw.t.u-tokyo.ac.jp
Homepage: http://www.bmw.t.u-tokyo.ac.jp/
S. Hattori, Dr. T. Ishii, T. Suma
Department of Bioengineering, The University of Tokyo
Hongo 7-3-1, Bunkyo-ku, Tokyo 113-8656 (Japan)
Dr. K. Miyata, S. Uchida
Division of Clinical Biotechnology, Center for Disease Biology and Integrative Medicine, The University of Tokyo
Hongo 7-3-1, Bunkyo-ku, Tokyo 113-0033 (Japan)
E-mail: miyata@bmw.t.u-tokyo.ac.jp
Dr. N. Nishiyama
Polymer Chemistry Division, Chemical Resources Laboratory
Tokyo Institute of Technology, R1-11
4259 Nagatsuta, Midori-ku, Yokohama 226-8503 (Japan)

[**] This research is supported by the Japan Society for the Promotion of Science (JSPS) through the "Funding Program for World-Leading Innovative R&D on Science and Technology (FIRST Program)," and Health and Labour Sciences Research Grants Research on Medical Device Development, Ministry of Health, Labour and Welfare. H.T. thanks the Research Fellowships of the Japan Society for the Promotion of Science for Young Scientists (JSPS).

Supporting information for this article is available on the WWW under http://dx.doi.org/10.1002/anie.201300178.

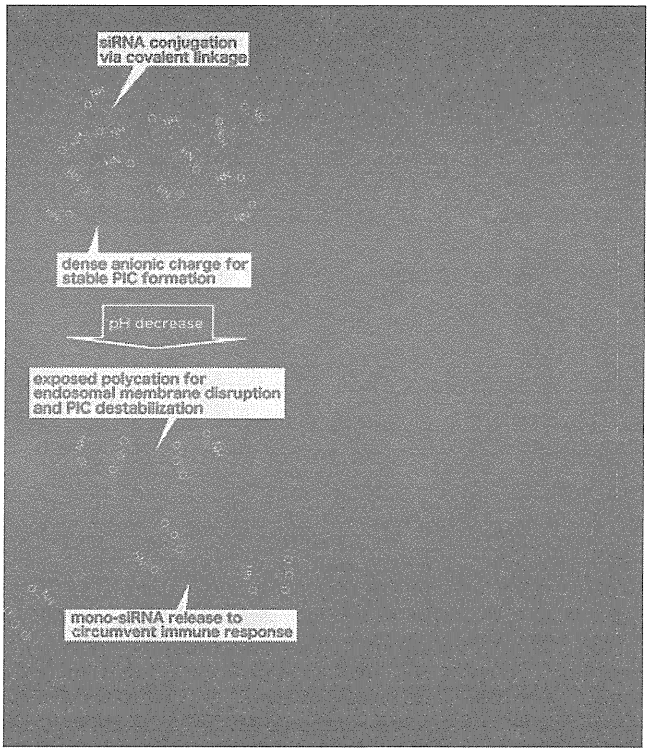

Figure 1. a) Illustration of releasable/enzyme-disrupting conjugate (REC) with the multifunctionality toward endosomal escape and release of mono-siRNA. b) Chemical structure of REC. c) Chemical structure of uREC. The PAsp derivative in this study has the mixed sequence of α and β isomers. Only α isomers are depicted in (b) and (c) for simplicity.

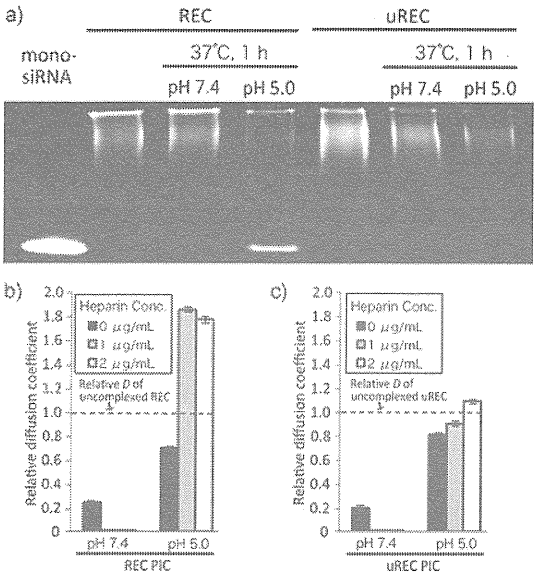

Figure 2. a) PAGE analysis of REC and uREC before and after 1 h incubation at 37 °C and at pH 7.4 or pH 5.0. b),c) Relative *D* values of siRNA conjugate PICs after a 30 min incubation at 37 °C with various heparin concentrations at pH 7.4 or pH 5.0. Relative *D* values are calculated by normalization of *D* to that of uncomplexed siRNA conjugates; REC PIC (b) and uREC PIC (c). Results were shown as mean and standard deviation obtained from 10 measurements.

effect of MAA linkage on the siRNA releasability, another siRNA conjugate, in which the DBCO group was directly conjugated to primary amines in PAsp(DET) without MAA linkage, was also synthesized as an siRNA-unreleasable but endosome-disrupting control (uREC; Figure 1c). The obtained siRNA conjugates were analyzed for their pH-sensitivity by polyacrylamide gel electrophoresis (PAGE) analysis (Figure 2a). The retarded bands in siRNA conjugates, compared to mono-siRNA, indicate that both siRNA conjugates had significantly higher molecular weight than mono-siRNA. A 1 h incubation of REC at pH 5.0 resulted in the band appearance at the same position as mono-siRNA, whereas such band was not observed at pH 7.4, indicating that mono-siRNA release was triggered selectively at the acidic pH. In contrast, the band corresponding to mono-siRNA was not observed for uREC after a 1 h incubation at both pHs of 5.0 and 7.4, indicating the essential role of MAA linkage for mono-siRNA release from REC.

Next, siRNA conjugates were mixed with a polycation PAsp(DET) to form PICs at N/P 10 (residual molar ratio of amines of PAsp(DET) to phosphates of siRNA) for their facilitated cellular uptake. PIC formation with siRNA conjugates as well as mono-siRNA was confirmed by fluorescence correlation spectroscopy (FCS) using Cy3-labeled siRNA (Cy3-siRNA) and its conjugates (Supporting Information, Table S2) as well as agarose gel electrophoresis (Supporting Information, Figure S6). The diffusion coefficients D in 10 mM HEPES buffer (pH 7.4) were determined to be 66.2 $\mu m^2 s^{-1}$ for mono-siRNA PIC and 2.9 $\mu m^2 s^{-1}$ for both siRNA conjugate PICs. These values were significantly smaller than those of the uncomplexed controls; that is, mono-siRNA (94.5 $\mu m^2 s^{-1}$) and siRNA conjugates (15.5 $\mu m^2 s^{-1}$ for REC and 18.8 $\mu m^2 s^{-1}$ for uREC). Considering that the D value of nanoparticles is inversely correlated with their size,[11] the smaller D values in the presence of polycation indicate successful PIC formation with the siRNA conjugates as well as mono-siRNA in the aqueous condition (siRNA concentration: 100 nM). The substantially smaller D values of the conjugate PICs, compared to the mono-siRNA PIC, indicate a larger association number of siRNA in the conjugate PICs, which is presumably due to increased anionic charges in the conjugate. Then, the acidic pH-sensitive PIC stability was further evaluated by FCS after a 30 min incubation of PICs at 37 °C in 10 mM HEPES (pH 7.4) and 10 mM MES (pH 5.0) containing heparin. Heparin is a major component of extracellular matrices on cellular surface and probably serves as a strong polyanionic counterpart to induce PIC dissociation.[12] The obtained D values of each sample were normalized to that of the corresponding uncomplexed siRNA control; that is, uncomplexed REC for REC PIC, uncomplexed uREC for uREC PIC, and uncomplexed mono-siRNA for mono-siRNA PIC (Figure 2b,c; Supporting Information, Figure S7, respectively). After incubation with heparin, a relative D of mono-siRNA PICs progressively increased with the increase in heparin concentration similarly at both pH values of 7.4 and 5.0, indicating that mono-siRNA PICs gradually dissociated with the increased counter polyanion, regardless of the environmental pH (Supporting Information, Figure S7). In contrast, relative D values of

REC and uREC PICs decreased after incubation with heparin at pH 7.4, suggesting that the conjugated siRNA is more stably encapsulated within PICs, compared to mono-siRNA, even after binding of heparin onto PIC surface. Notably, the incubation of REC and uREC PICs at pH 5.0 dramatically increased their relative *D* values, and furthermore, the increase in the relative *D* values was facilitated in the presence of heparin, indicating the acidic pH-responsive destabilization of the siRNA conjugate PICs (Figure 2b,c). Considering the fact that the MAA linkage contained in both siRNA conjugates can degrade at pH 5.0 to generate the polycations in PIC, the destabilization of siRNA conjugate PICs at pH 5.0 is presumably due to the electrostatic repulsion between the generated polycations and the originally incorporated polycations in PIC. Furthermore, the increased relative *D* values of REC PICs in the presence of heparin, beyond that of uncomplexed REC, strongly suggest the mono-siRNA release triggered by the cleavage of MAA linkage. These results demonstrate that the acidic pH-sensitivity of the MAA-based conjugates can be maintained even after PIC formation, and also they provide siRNA PICs with a reversible stability in response to the intracellular environment.

Delivery functionalities of REC PICs, namely cellular uptake efficiency and intracellular trafficking profile, were evaluated with cultured human ovarian cancer cells stably expressing luciferase (SKOV3-Luc). Cellular uptake of siRNA was estimated using Cy3-siRNA with a fluorescence microscopy (Supporting Information, Figure S8). REC and uREC PICs (N/P 10) allowed 30% increase in Cy3 fluorescence from cells compared to mono-siRNA PICs (N/P 10, $p < 0.005$), indicating that the conjugate formulation significantly enhanced the cellular uptake of siRNA is probably due to the higher stability, as suggested by the FCS result at pH 7.4 (Figure 2b,c; Supporting Information, Figure S7). Next, confocal laser scanning microscopic (CLSM) observation was performed to examine subcellular distribution of siRNA PICs (N/P 10), especially focusing on the colocalization of siRNA with the late endosome/lysosome as an indicator for endosomal entrapment (Figure 3a–c).[13] In the cells treated with mono-siRNA PICs, the colocalization (yellow) ratio of Cy3-siRNA (red) with a late endosome/lysosome marker LysoSensor Green (green) was increased up to 70% for the initial 12 h and then kept constant for subsequent 36 h (Figure 3d). In contrast, the cells treated with REC and uREC PICs showed that the colocalization ratio was progressively decreased over incubation period and reached about 30% after a 48 h incubation. The significantly lower colocalization ratios (or less endosomal entrapment) of REC/uREC PICs strongly suggest more efficient endosomal escape of siRNA compared to mono-siRNA PICs (Figure 3d). This enhanced endosomal escape with REC and uREC is consistent with the endosome-disrupting functionality of the backbone polymer, which should be converted into the parent polycation PAsp(DET) in the acidic late endosome/lysosome for the membrane disruption, as suggested by a membrane disruption assay at pH 7.4 and 5.0 (Supporting Information, Figure S9).[8,9]

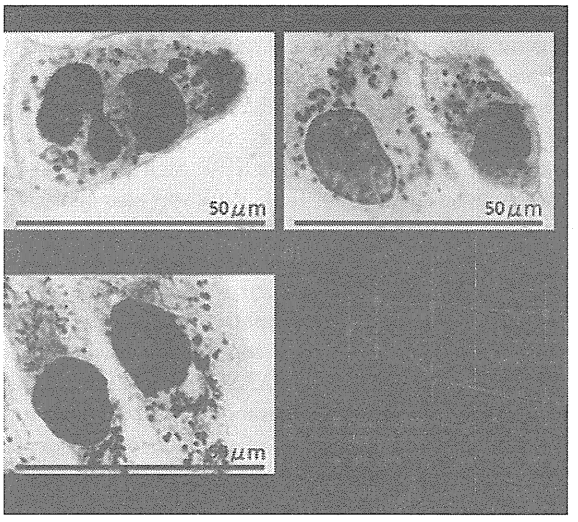

Figure 3. a–c) CLSM images 48 h after treatment of SKOV3-Luc cells with mono-siRNA PIC (a), REC PIC (b), and uREC PIC (c). Red Cy3-siRNA, green late endosome/lysosome (LysoSensor Green), blue nucleus (Hoechst 33342). A yellow pixel indicates colocalization between a red pixel and green pixel. d) Time-dependent change in the colocalization ratio between Cy3-siRNA and late endosome/lysosome. The colocalization ratio was shown as mean and standard deviation obtained from 10 cells. The *p* value was calculated according to Student's *t* test.

Next, the gene silencing ability of REC PICs was compared with mono-siRNA and uREC PICs by luciferase assay with cultured SKOV3-Luc cells (Figure 4a). Obviously, REC and uREC PICs achieved more efficient sequence-specific gene silencing in the cells than mono-siRNA PICs, which is presumably due to the enhanced endosomal escape of siRNA conjugate PICs (Figure 3) as well as facilitated cellular uptake of siRNA (Supporting Information, Figure S8). Interestingly, REC PICs induced significantly stronger gene silencing than uREC PICs ($p < 0.005$), demonstrating the positive effect of siRNA releasability by the MAA linkage on the siRNA delivery functionality. Mono-siRNA

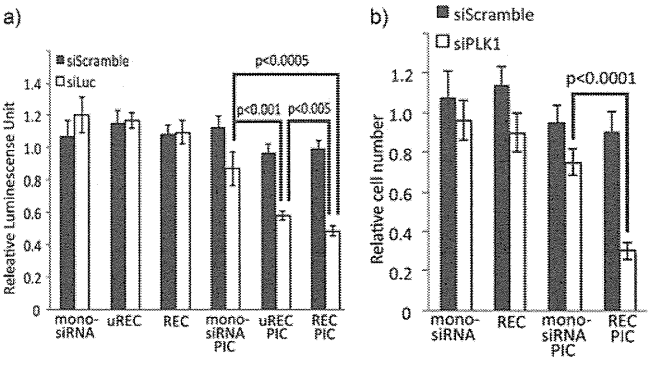

Figure 4. a) Luciferase gene expression in cultured SKOV3-Luc cells after PIC treatment at 100 nM Luc siRNA (siLuc) or scramble siRNA (siScramble) for 48 h. b) Cell viability in cultured A549 cells after PIC treatment at 100 nM PLK1 siRNA (siPLK1) or siScramble for 72 h. In both figures, results were shown as mean and standard deviation obtained from 6 samples. The *p* values were calculated according to Student's *t* test.

releasates from REC might be more readily associated with the gene silencing pathway owing to compromised steric hindrance compared to the conjugated structure. Also, no cytotoxicity was observed for all the tested PIC formulations under the same conditions as the gene-silencing assay (Supporting Information, Figure S10). Significantly stronger luciferase gene silencing of REC PICs was also confirmed in comparison with mono-siRNA PICs prepared with PAsp(DET)/PAsp(DET-CDM) (a non-covalent control) and a commercially available reagent ExGen500 (linear polyethylenimine; Supporting Information, Figure S11), demonstrating the advantage of REC formulation, including covalent conjugation between siRNA and the backbone polymer. The effect of the siRNA-releasability of REC was further examined from the standpoint of immune responses; IFNα response was determined as an indicator of immune response by enzyme-linked immunosorbent assay (ELISA). REC, uREC, and their PICs did not induce a detectable level of IFNα production for SKOV3-Luc cells ($< 10\,pg\,mL^{-1}$, data not shown). Thus, the similar ELISA experiment was further challenged for murine macrophage cells (Raw264.7), which are known to be highly sensitive to immunogen.[14] As a result, REC PICs induced a significantly lower level of IFNα production ($24.3 \pm 3.5\,pg\,mL^{-1}$) compared to uREC PICs ($60.8 \pm 12.9\,pg\,mL^{-1}$, $p < 0.005$), indicating that the siRNA-releasability based on MAA linkage successfully decreased the immune response for siRNA conjugates. Uncomplexed REC and uREC without polycation did not induce a detectable level of IFNα production, suggesting that they should not stimulate IFNα response at least on the cellular surface. Finally, the utility of REC PICs was verified for other cell lines, using a therapeutic siRNA targeting polo-like kinase 1 (PLK1). PLK1 is known to be a cell cycle regulator, and thus its silencing can arrest the cell cycle toward the apoptosis.[15] REC PICs with PLK1 siRNA (N/P 20) sequence-specifically suppressed the growth of human lung carcinoma cells (A549) and human hepatocarcinoma cells (Huh-7; Figure 4b; Supporting Information, Figure S12, respectively), demonstrating a strong potential of the REC formulation bearing the MAA linkage for siRNA-based cancer therapy.

In summary, an acidic pH-responsive siRNA conjugate was developed for enhanced siRNA delivery with reduced immunogenicity. A single chemical process based on the MAA linkage successfully provided the multifunctionality required for successful siRNA delivery; that is, reversible carrier stability, endosomal escapability, and mono-siRNA releasability. Ultimately, the siRNA conjugate sequence-specifically achieved the significant growth inhibition of cancerous cells. The programmed siRNA delivery based on the smart conjugate will be further investigated for the success in siRNA therapeutics.

Received: January 9, 2013
Revised: February 25, 2013
Published online: April 29, 2013

Keywords: conjugation · drug delivery · drug design · polymers · siRNA

[1] a) S. M. Elbashir, J. Harborth, W. Lendeckel, A. Yalcin, K. Weber, T. Tuschl, *Nature* **2001**, *411*, 494–498; b) J. C. Burnett, J. J. Rossi, *Chem. Biol.* **2012**, *19*, 60–71.

[2] R. L. Kanasty, K. A. Whitehead, A. J. Vegas, D. G. Anderson, *Mol. Ther.* **2012**, *20*, 513–524.

[3] a) D. B. Rozema, D. L. Lewis, D. H. Wakefield, S. C. Wong, J. J. Klein, P. L. Roesch, S. L. Bertin, T. W. Reppen, Q. Chu, A. V. Blokhin, J. E. Hagstrom, J. A. Wolf, *Proc. Natl. Acad. Sci. USA* **2007**, *104*, 12982–12987; b) Y. Singh, P. Murat, E. Defrancq, *Chem. Soc. Rev.* **2010**, *39*, 2054–2070; c) M. R. Alam, X. Ming, M. Fisher, J. G. Lackey, K. G. Rajeev, M. Manoharan, R. L. Juliano, *Bioconjugate Chem.* **2011**, *22*, 1673–1681; d) S. K. Lee, A. Siefert, J. Beloor, T. M. Fahmy, P. Kumar, *Methods Enzymol.* **2012**, *502*, 91–122.

[4] a) A.-L. Bolcato-Bellemin, M.-E. Bonnet, G. Creusat, P. Erbacher, J.-P. Behr, *Proc. Natl. Acad. Sci. USA* **2007**, *104*, 16050–16055; b) H. Mok, S. H. Lee, J. W. Park, T. G. Park, *Nat. Mater.* **2010**, *9*, 272–278; c) H. Takemoto, A. Ishii, K. Miyata, M. Nakanishi, M. Oba, T. Ishii, Y. Yamasaki, N. Nishiyama, K. Kataoka, *Biomaterials* **2010**, *31*, 8097–8105; d) C. A. Hong, S. H. Lee, J. S. Kim, J. W. Park, K. H. Bae, H. Mok, T. G. Park, H. Lee, *J. Am. Chem. Soc.* **2011**, *133*, 13914–13917; e) S. J. Lee, M. S. Huh, S. Y. Lee, S. Min, S. Lee, H. Koo, J. U. Chu, K. E. Lee, H. Jeon, Y. Choi, K. Choi, Y. Byun, S. Y. Jeong, K. Park, K. Kim, I. C. Kwon, *Angew. Chem.* **2012**, *124*, 7315–7319; *Angew. Chem. Int. Ed.* **2012**, *51*, 7203–7207.

[5] A. Judge, I. MacLachlan, *Hum. Gene Ther.* **2008**, *19*, 111–124.

[6] a) C. Troiber, E. Wagner, *Bioconjugate Chem.* **2011**, *22*, 1737–1752; b) J. Nguyen, F. C. Szoka, *Acc. Chem. Res.* **2012**, *45*, 1153–1162.

[7] a) D. B. Rozema, K. Ekena, D. L. Lewis, A. G. Loomis, J. A. Wolff, *Bioconjugate Chem.* **2003**, *14*, 51–57; b) S. Guo, Y. Huang, Q. Jiang, Y. Sun, L. Deng, Z. Liang, Q. Du, J. Xing, Y. Zhao, P. C. Wang, A. Dong, X.-J. Liang, *ACS Nano* **2010**, *4*, 5505–5511.

[8] Y. Lee, K. Miyata, M. Oba, T. Ishii, S. Fukushima, M. Han, H. Koyama, N. Nishiyama, K. Kataoka, *Angew. Chem.* **2008**, *120*, 5241–5244; *Angew. Chem. Int. Ed.* **2008**, *47*, 5163–5166.

[9] K. Miyata, M. Oba, M. Nakanishi, S. Fukushima, Y. Yamasaki, H. Koyama, N. Nishiyama, K. Kataoka, *J. Am. Chem. Soc.* **2008**, *130*, 16287–16294.

[10] H. Takemoto, K. Miyata, T. Ishii, S. Hattori, S. Osawa, N. Nishiyama, K. Kataoka, *Bioconjugate Chem.* **2012**, *23*, 1503–1506.

[11] J. DeRouchey, C. Schmidt, G. F. Walker, C. Koch, C. Plank, E. Wagner, J. O. Radler, *Biomacromolecules* **2008**, *9*, 724–732.

[12] a) M. J. Palte, R. T. Raines, *J. Am. Chem. Soc.* **2012**, *134*, 6218–6223; b) M. Zheng, D. Librizzi, A. Kılıç, Y. Liu, H. Renz, O. M. Merkel, T. Kissel, *Biomaterials* **2012**, *33*, 6551–6558.

[13] K. Whitehead, G. Sahay, G. Z. Li, K. T. Love, C. A. Alabi, M. Ma, C. Zurenko, W. Querbes, R. S. Langer, D. G. Anderson, *Mol. Ther.* **2011**, *19*, 1688–1694.

[14] J. Turco, H. H. Winker, *Infect. Immun.* **1982**, *35*, 783–791.

[15] a) A. D. Judge, M. Robbins, I. Tavakoli, J. Levi, L. Hu, A. Fronda, E. Ambegia, K. McClintock, I. MacLachlan, *J. Clin. Invest.* **2009**, *119*, 661–673; b) K. Strebhardt, *Nat. Rev. Drug Discovery* **2010**, *9*, 643–660.

Journal of Controlled Release 167 (2013) 238–247

Contents lists available at SciVerse ScienceDirect

Journal of Controlled Release

journal homepage: www.elsevier.com/locate/jconrel

Block/homo polyplex micelle-based GM-CSF gene therapy *via* intraperitoneal administration elicits antitumor immunity against peritoneal dissemination and exhibits safety potentials in mice and cynomolgus monkeys

Masahiro Ohgidani [a], Koichi Furugaki [a], Kentaro Shinkai [b], Yumi Kunisawa [a], Keiji Itaka [c], Kazunori Kataoka [c,d], Kenji Nakano [a,*]

[a] *Innovation Center for Medical Redox Navigation, Kyushu University, 3-1-1 Maidashi, Higashi-ku, Fukuoka 812-8582, Japan*
[b] *Department of Cancer Research and Therapy, Graduate School of Medical Sciences, Kyushu University, 3-1-1 Maidashi, Higashi-ku, Fukuoka 812-8582, Japan*
[c] *Division of Clinical Biotechnology, Center for Disease Biology and Integrative Medicine, Graduate School of Medicine, The University of Tokyo, 7-3-1 Hongo, Bunkyo-ku, Tokyo 113-0033, Japan*
[d] *Department of Materials Engineering, Graduate School of Engineering, The University of Tokyo, 7-3-1 Hongo, Bunkyo-ku, Tokyo 113-0033, Japan*

ARTICLE INFO

Article history:
Received 18 October 2012
Accepted 6 February 2013
Available online 17 February 2013

Keywords:
Block/homo polyplex micelle
Intraperitoneal administration
Immunogene therapy
Granulocyte macrophage colony stimulating factor
Peritoneal dissemination
Safety evaluation test in cynomolgus monkeys

ABSTRACT

A block/homo-mixed polyplex micelle, comprising of cationic homo polymer: poly{N′-[N-(2-aminoethyl)-2-aminoethyl]aspartamide} P[Asp(DET)] and block copolymer: polyethylene glycol (PEG)-*b*-P[Asp(DET)], has been reported to exhibit the efficient transgene expression *in vivo* by intratracheal and systemic administration. In the present study, we investigated the potential of immunogene therapy by intraperitoneal (i.p.) administration of block/homo polyplex micelles for peritoneal dissemination. For evaluation of transgene expression *in vivo*, block/homo polyplex micelles showed 12-fold higher level in luciferase expression evaluated by bioluminescence imaging system at 24 h after the i.p. administration compared with block polyplex micelles composed with only PEG-*b*-P[Asp(DET)] in nude mice bearing peritoneal dissemination. The distribution of block/homo polyplex micelles and intracellular uptake of pDNA was observed in tumor nodules. The tumor growth and the prolonged survival rate for the mice harboring disseminated pancreatic cancer more significantly compared with the mock. The antitumor effect of GM-CSF gene therapy was mediated *via* the activation of natural killer cells. For safety evaluation, block/homo polyplex micelles indicated almost no adverse events for patho-physical findings and blood examinations in mice and cynomolgus monkeys, although slight increases in serum fibrinogen were observed in the monkey model. In conclusion, block/homo polyplex micelle-based immunogene therapy *via* i.p. administration may be a safe and effective approach for suppressing intractable peritoneal dissemination.

1. Introduction

Gene therapy has been extensively explored for a promising approach to overcome the limitation of conventional treatments against refractory diseases, such as genetic disorders, neurodegenerative disease and cancer [1,2]. Viral gene vectors, such as adenovirus, adeno-associated virus and lentivirus vector, have been applied in clinical trials of gene therapy due to the property of high efficient transduction [3]; however, their use for clinical application is limited due to the safety concerns. Accordingly, the development of several lines of non-viral gene carriers, such as synthetic polymer micelles and liposomes [4,5], has been addressed due to the industrial aspects of production and pathogen-free properties [6].

As a candidate synthetic material of non-viral gene carrier, a cationic polymer, poly{N′-[N-(2-aminoethyl)-2-aminoethyl]aspartamide} (P[Asp(DET)]), has been developed by Kataoka and co-colleagues [7–10]. Basic structure of P[Asp(DET)] has two advantages: pH-responsible protonation, which enhances the escape from endosome [7], and the biodegradability under physiological conditions, which minimizes the cumulative toxicity [8]. However, the use of P[Asp(DET)] homo polymer has limited potentials in biocompatibility *in vivo* by own cationic charge, because of strong interaction with charged components and high clearance by reticuloendothelial system (RES). To resolve the problem, polyethylene glycol (PEG)-conjugated block copolymer, PEG-*b*-P[Asp(DET)] with low cytotoxicity and prolonged blood circulation, has been prepared [7,8,10–13], although transgene expression of the block copolymer micelles is drastically reduced compared with homo polymer micelles. Therefore, a block copolymer integrated disulfide linkage (SS) between P[Asp(DET)] and PEG {PEG-SS-P[Asp(DET)]} has been designed [14] to achieve the efficient gene transduction by detaching PEG shields from the core of polymer in the reducing environment of the endosomal compartments [14,15]. However, PEG-SS-P[Asp(DET)] is supposed to be difficult to synthesize and preserve, especially in good manufacturing practice (GMP) grade, due to the less stability of this copolymer. Instead, novel strategy was recently emerged: block/homo mixed polyplex micelles comprising of PEG-*b*-P[Asp(DET)] and P[Asp(DET)], which represent

* Corresponding author. Tel.: +81 92 642 6209; fax: +81 92 642 6024.
E-mail address: kenakano@med.kyushu-u.ac.jp (K. Nakano).

0168-3659/$ – see front matter © 2013 Elsevier B.V. All rights reserved.
http://dx.doi.org/10.1016/j.jconrel.2013.02.006

high potentials of transfection activity and safety by systemic and intratracheal administration [16,17].

Peritoneal dissemination, a most intractable metastasis of advanced cancers, has relative resistance to systemic chemotherapy due to peritoneal–plasma barrier for effective transport of anti-cancer drugs from blood circulations into the peritoneal lesions [18]. Alternatively, intraperitoneal (i.p.) administration of drugs has some advantages against intraperitoneally disseminated tumors compared to systemic administration [19,20], because the drugs are directly delivered and retarded into peritoneal cavity, resulting in high dose concentration in tumor tissues [21]. In addition, gene therapy continuously produces therapeutic molecules, such as cytokines and bioactive peptides, and compensates their rapid clearance by enzymatic degradation. We hypothesize the pharmacological advantages of i.p. administered PEG-*b*-P[Asp(DET)]/P[Asp(DET)] (block/homo) polyplex micelles for the transduction of therapeutic genes against peritoneal disseminated cancer. However, the antitumor efficacy and safety reserve of gene therapy *via* i.p. administration of block/homo polyplex micelles remain unknown.

In this study, we demonstrated the antitumor efficacy of gene therapy by i.p. administration of PEG-*b*-P[Asp(DET)]/P[Asp(DET)] (block/homo) polyplex micelles encapsulating granulocyte macrophage colony stimulating factor (GM-CSF) gene in mice with peritoneal dissemination of pancreatic cancer. We also confirmed the safety potentials of block/homo polyplex micelle in mice and cynomolgus monkeys. Immunogene therapy *via* i.p. administration of block/homo polyplex micelles may be a promising strategy to suppress the progression of peritoneally disseminated cancers.

2. Materials and methods

2.1. Plasmid DNA construction

A plasmid encoding luciferase (pCpG-ΔLuc) was kindly supplied from Dr. Makiya Nishikawa (Kyoto University) [22]. As expression plasmids encoding therapeutic gene, pVIVO-mGM-CSF was constructed as follows; the open-reading frame of mouse GM-CSF was integrated at the multi-cloning sites in the plasmid DNA of pVIVO1-mcs with hamster 78-kDa glucose-regulated protein (GRP78) promoter which yields persistent high expression within the tumor micro-environment. Plasmid of pCpG-mcs (mock) was used as a control (Invivogen, San Diego, CA). The plasmid DNA was amplified in competent DH5A *Escherichia coli* cells and purified using EndoFree Plasmid Giga Kit (QIAGEN Inc., Valencia, CA).

2.2. Preparation of polyplex micelles encapsulating pDNA

Block copolymer PEG-*b*-P[Asp(DET)] (Mw of PEG: 12,000; DP of P[Asp(DET)] segment: 65) and homo polymer P[Asp(DET)] (segment: 55) synthesized as previously reported [7–9] were kindly provided from NOF corp. (Kawasaki, Japan). Polyplex micelles encapsulating pDNA were prepared by mixing pDNA (50 or 100 μg), PEG-*b*-P[Asp(DET)] and P[Asp(DET)] in 10 mM HEPES buffer (pH 7.3) at the block copolymer/homo polymer ratio of 7/3 and the N/P ratio (N = total amines in polycations; P = total phosphate anions in pDNA) of 10.

2.3. Dynamic light scattering (DLS) and ζ-potential measurements

DLS and ζ-potential measurements were carried out at 25 °C using an ELSZ-SV2 (Otsuka Electronics Co., Ltd., Osaka, Japan), equipped with a He–Ne ion laser (633 nm) as the incident beam. For measurement of micelle size, the light scattering data were obtained with a detection angle of 160° at 25 °C. The rate of decay in the photon correlation function was analyzed by the cumulant method, and the corresponding hydrodynamic diameter of the polyplexes was then calculated by the Stokes–Einstein equation. The ζ-potential of micelles was calculated from the obtained electrophoretic mobility by the Smoluchowski equation: $\zeta = 4\pi\eta\upsilon/\varepsilon$, where η is the viscosity of the solvent, υ is the electrophoretic mobility and ε is the dielectric constant of the solvent.

2.4. Cell lines

Human pancreatic carcinoma SUIT-2 and mouse lymphoma YAC-1 were obtained from the American Type Culture Collection. SUIT-2, SUIT-2 stably expressing luciferase (SUIT-2/Luc) as previously established [15] and YAC-1 cells were cultured in RPMI1640 medium (Nacalai Tesque, Ltd.) supplemented with 10% heat-inactivated fetal bovine serum (FBS, Wako Pure Chemical Industries, Ltd.), 100 U/mL penicillin and 100 μg/mL streptomycin at 37 °C in humidified incubators containing 5% CO_2.

2.5. Animals

BALB/c nude mice (CAnN.Cg-Foxn1<nu>/CrlCrlj) and BALB/cAnNCrlCrlj mice (female, 6 weeks old) were purchased from Charles River Laboratories (Yokohama, Japan). Animals were housed in a temperature-controlled room under 12/12 h light/dark cycles and accessed the intake of food and water *ad libitum*. Animal experiments were approved and carried out in compliance with the Guidelines for Animal Experiments of Kyushu University from the Animal Care and Use Committee at Kyushu University.

2.6. In vivo luminescence analysis for transgene expression

BALB/c nude mice were intraperitoneally inoculated with SUIT-2 cells (1×10^6 cells/mouse). One week later, polyplex micelles consisting of 100 μg of pCpG-ΔLuc were administered intraperitoneally. Bioluminescent signals were analyzed with an IVIS imaging system (Xenogen Biosciences, Alameda, CA) using Living Image software (Xenogen Biosciences). At twenty minutes prior to determination, animals intraperitoneally received the substrate D-Luciferin solution (Summit Pharmaceuticals International Corporation, Tokyo, Japan) at 75 mg/kg under anesthesia with the inhalation of 2.5% isoflurane (Abbot Laboratories, North Chicago, IL).

2.7. Analysis for distribution of block/homo polyplex micelles

Fluolid Orange NHS (International Science Technology Co. LTD., Fukuoka, Japan) was conjugated to amino groups of PEG-*b*-P[Asp(DET)] according to the manufacturer's instruction. BALB/c nude mice were intraperitoneally inoculated with SUIT-2/Luc cells (1×10^6 cells/mouse). Tumors were allowed to grow for one week. Fluolid-labeled polyplex micelles loading pDNA (50 μg/mouse) were intraperitoneally injected. Tumor, liver, spleen and lymph node tissues were obtained, embedded and frozen in OCT compounds at 24 h after injection of Fluolid-labeled micelles. Frozen sections (8–10 μm) were air-dried and fixed in cold acetone for 10 min. The nuclei were stained with 4′,6-diamidino-2-phenylindole (DAPI). The Fluolid signal of polyplexes was observed by confocal laser scanning microscopy NIKON A1 (Nikon Corporation, Tokyo, Japan).

2.8. Analysis for cellular uptake of pDNA in tumor tissue

Fluorescence-labeled pDNA was prepared using Label IT Cy5 labeling kit (Mirus, Madison, WI) according to the manufacturer's instructions. In the above model of BALB/c nude mice, block/homo polyplex micelles with Cy5-labeled pCpG-ΔLuc (50 μg; N/P ratio = 10) were administered into the peritoneal cavity of nude mice. Tumor tissues were obtained at 24 h after administration of polyplex micelles and the distribution of Cy5-labeled pDNA was examined by confocal laser scanning microscopy as described above.

2.9. Antitumor activity of mGM-CSF gene therapy for peritoneal dissemination

BALB/c nude mice (n = 8 in each group) were intraperitoneally inoculated with SUIT-2/Luc cells (2×10^5 cells/mouse). Tumors were allowed to grow for one week. Subsequently, block/homo polyplex micelles with mGM-CSF (50 μg; N/P ratio = 10) or mock (50 μg; N/P ratio = 10) were administered three-times with every one week interval into the peritoneal cavity of mice. *In vivo* bioluminescent signals were analyzed with an IVIS imaging system as described above to assess the amount of disseminated tumor. The survival of the mice was also monitored in each group until 135 days after the initial inoculation of block/homo polyplex micelles.

2.10. Quantitative real-time reverse-transcriptional PCR (qRT-PCR) for mGM-CSF mRNA expression

The expression of mGM-CSF mRNA in tumor and normal organ tissues was evaluated by qRT-PCR. At several time points (days 1, 2, 4 and 7) after the injection of block/homo polyplex micelles with mGM-CSF or mock pDNA, tumor and other organ tissues (spleen, liver, kidney, lung and intestine) were snap-frozen in liquid nitrogen and kept at −80 °C for the following assays. Total RNA was extracted using illustra™ RNAspin Mini RNA Isolation Kit (GE Healthcare UK, Ltd., Buckinghamshire, UK) according to the manufacturer's instruction, and subjected to cDNA synthesis using Transcriptor First Strand cDNA Synthesis Kit (Roche Applied Science, Mannheim, Germany). qRT-PCR for mGM-CSF and β-actin as a house-keeping control gene was performed using mGM-CSF primers: 5′-TCGAATTCTGTACAGCATGCAGCTC-3′ and 5′-GCCAGAGGGCTGATTAG AGA-3′; β-actin primers of Universal ProbeLibrary Set (Roche Applied Science) in the LightCycler 480 II System (Roche Diagnostics, Mannheim, Germany).

2.11. Immunohistochemistry for mGM-CSF protein expression

Tissue samples were obtained, embedded and frozen in OCT compounds at 24 h after injection of block/homo polyplex micelles. Frozen sections (8–10 μm) were air dried and fixed in cold acetone for 10 min. After blocking with 3% bovine serum albumin (BSA), the sections were incubated with a rat anti-mouse GM-CSF antibody (1:1000; Abcam, Cambridge, MA) at room temperature for 1 h, followed by a biotinylated rabbit anti-rat IgG (H + L) (1:250; Vector Laboratories Inc., Burlingame, CA) at room temperature for 1 h. The samples were incubated with horseradish peroxidase-conjugated streptavidin (PK-6100, Vector Laboratories Inc., Burlingame, CA), followed by staining with 3,3′-diaminobenzidine (DAB) substrate (SK-4100, Vector Laboratories Inc.).

2.12. Analysis for NK cytotoxicity of mGM-CSF immune gene therapy

NK cytotoxicity was measured by cell killing assay of YAC-1 cell as target cells [23]. As effector cells, splenocytes from the mice at day 7 after the injection of saline, mock or mGM-CSF block/homo polyplex micelles were used. YAC-1 cells (2×10^6 cells/mL) were labeled with 10 μM 5- or 6-(N-Succinimidyloxycarbonyl)-fluorescein-3′,6′-diacetate (CFSE; Dojindo Inc., Kumamoto, Japan) at 37 °C for 10 min, followed by stopping the reaction with equal volume of FBS at room temperature for 2 min. Cells were washed in PBS and resuspended in RPMI1640 medium including FBS, penicillin and streptomycin. Splenocytes from the mice treated with saline, mock or mGM-CSF gene therapy were washed and resuspended in RPMI1640 medium. Both cells were mixed in the ratios of effector to target (25:1, 50:1 or 100:1) and incubated in humidified atmosphere of 5% CO_2 at 37 °C for 6 h. Propidium iodide (1 μg/mL; Nacalai Tesque Inc., Kyoto, Japan) and Flow-Count Fluorospheres (10,000 beads; Coulter Corporation, Miami, FL) were added to the mixed cells prior to flow cytometer analysis (FACS Cant II, Becton Dickinson Inc.). The percentage of target cell viability (%) was calculated as follows: Viability (%) = (CFSE positive cells treated with splenocytes / CFSE positive cells without splenocytes) × 100.

2.13. Assessment of toxicity of block/homo polyplex micelles after i.p. administration in mice

Block/homo polyplex micelles loaded with pVIVO-mGM-CSF or mock (50 μg/mouse, N/P ratio = 10) were intraperitoneally administered to BALB/c mice (n = 5). Blood samples were collected from the vena cava in mice under anesthesia at 24 and 72 h. White blood cells (WBC), red blood cells (RBC), hematocrit (HCT) and platelet (PLT) were counted using multiple automatic blood cell county device (KX-21, Sysmex Co., Kobe, Japan). Creatinine, alanine aminotransferase (ALT), aspartate aminotransferase (AST), lactate dehydrogenase (LDH) and total bilirubin were determined by Japan Society of Clinical Chemistry (JSCC) methods with 7180 Clinical Analyzer (Hitachi, Tokyo, Japan). We also monitored body weight for 7 days post-administration as an index of influence for whole body.

2.14. Assessment of toxicity of block/homo polyplex micelles after i.p. administration in cynomolgus monkeys

Because mouse GM-CSF has no reactivity in cynomolgus monkeys, a safety evaluation in cynomolgus monkeys was performed using the block/homo polyplex micelles loaded with mock pDNA at Bozo Research Center, Inc. (Tokyo, Japan). Block/homo polyplex micelles consisting of

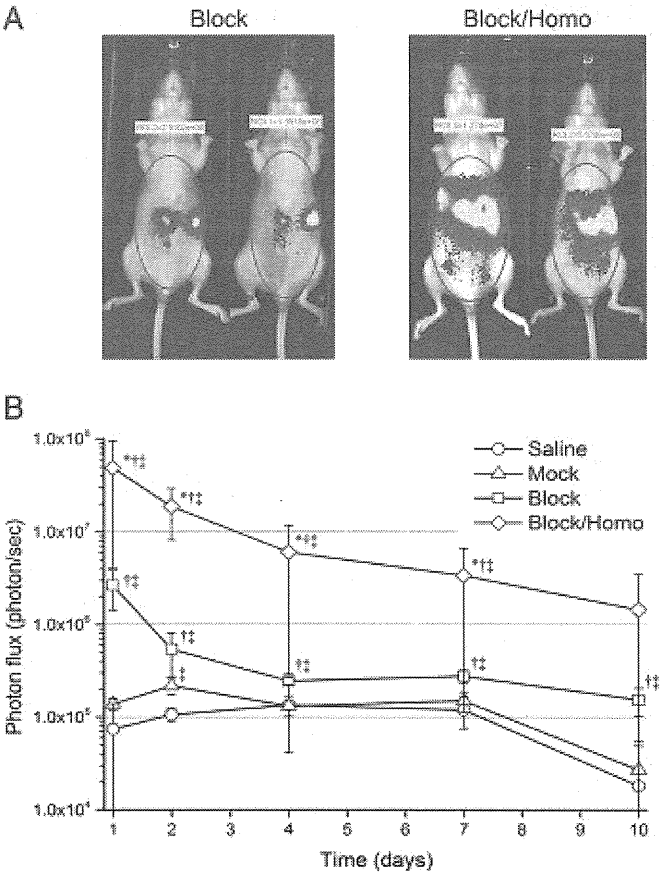

Fig. 1. *In vivo* transgene expression after i.p. administration of polyplex micelles. (A) Luciferase signals were analyzed with an IVIS imaging system at 24 h after i.p. administration of PEG-*b*-P[Asp(DET)] block or PEG-*b*-P[Asp(DET)]/P[Asp(DET)] block/homo polyplex micelles with a luciferase pDNA in nude mice harboring pancreatic SUIT-2 disseminated cancer. (B) Time-course changes in luciferase expression *in vivo* were evaluated with an IVIS imaging system. Saline (○); mock (△); block (◇); block/homo (□). Results are represented as means ± SD (n = 5; *$p<0.05$ *versus* block; †$p<0.05$ *versus* mock; ‡$p<0.05$ *versus* saline).

mock pDNA (1 mg/5 kg, 3 mg/5 kg or 10 mg/5 kg; N/P ratio = 10) were intraperitoneally administrated to cynomolgus monkeys aged 3–5 years (male and female n = 2 each; 2.5–4.8 kg body weight). Food consumption, general conditions and body weight of animals were observed for 7 days after the polyplex micelle administration. Blood samples (1 mL per time point) were collected at 24 h after each-dose injection of block/homo polyplex micelles. Blood hematology tests were performed using a multiple automatic blood cell county device (ADVIA120, Siemens Healthcare Diagnosis Inc., Deerfield, IL). Blood coagulation tests were performed using automatic blood coagulation analyzer (ACS Elite Pro, Instrumentation Laboratory Inc., Bedford, MA). Blood chemistry tests were performed by automatic clinical chemistry analyzer (TBA-120FR, Toshiba Medical Systems Corp., Tochigi, Japan). The animals were sacrificed at day 7 after injection of maximal-dose polyplex micelles, and tissue injuries of extirpated organs were examined.

2.15. Statistical analysis

Results are represented as means ± standard deviation (SD). Statistical analysis for data between two groups was performed using Student's t-test. Survival rate was estimated by Kaplan–Meier method and analyzed using a log-lank test. p values less than 0.05 were considered statistical significance.

3. Results

3.1. Polyplex micelle characterization

The polyplexes mixed with PEG-*b*-P[Asp(DET)], P[Asp(DET)] and pDNA (50 μg) (block/homo = 7/3, NP = 10) formed the micelles in diameter at 90.2 ± 2.05 nm, while those from PEG-*b*-P[Asp(DET)] and pDNA (50 μg) (NP = 10) at 101.5 ± 4.37 nm. The respective polyplex micelles showed neutral ζ-potential values at 5.91 and 5.46 mV.

3.2. Time-course analysis for transgene (luciferase) expression in vivo

Fig. 1 shows the time-course changes in expression efficiency *in vivo* after i.p. injection of polyplex micelles with a reporter luciferase gene. The luciferase activities for PEG-*b*-P[Asp(DET)]/P[Asp(DET)] block/homo and PEG-*b*-P[Asp(DET)] block polyplex micelles were elevated with the peak at 24 h and gradually declined thereafter, but still sustained on day 7 more than the mock and saline groups. Comparing the level of expression between the two polyplex micelles, the block/homo system exhibited 19-fold higher luciferase activity (4.9×10^7 photons/s) than the block system (2.6×10^5 photons/s, $p<0.05$) on day 1 after polyplex micelle injection. The luciferase activity was still higher in the block/homo (3.4×10^6 photons/s) than the block (2.8×10^5 photons/s) polyplex

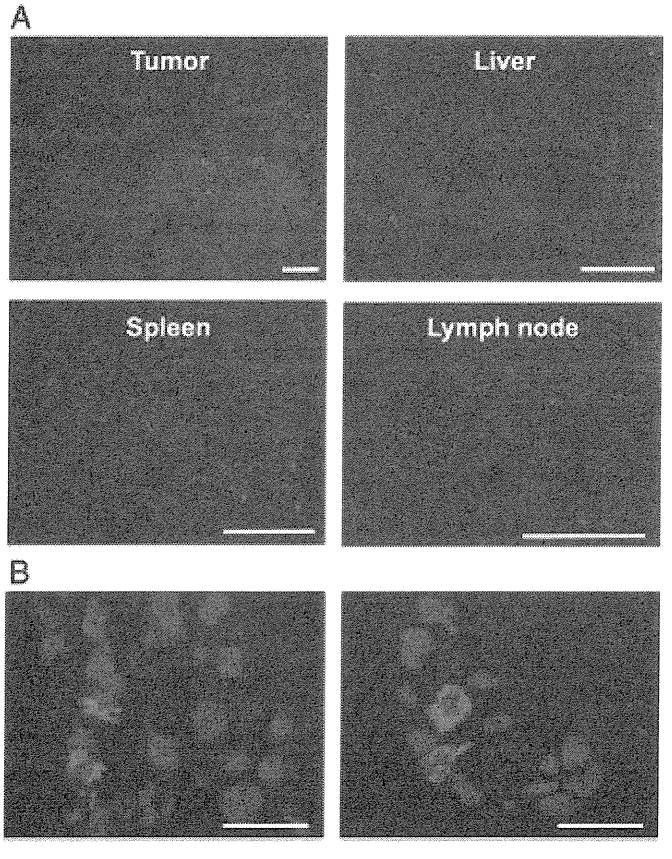

Fig. 2. *In vivo* distribution of block/homo polyplex micelles with Fluolid-labeled block copolymer and Cy5-labeled pDNA. Tissue samples were obtained from nude mice with SUIT-2/Luc peritoneal dissemination at 24 h after i.p. administration of block/homo polyplex micelles with pDNA, of which block copolymer or pDNA was labeled with Fluolid (A) or Cy5 (B), respectively. The fluorescent signals of polymer and pDNA in tissue sections were observed by confocal laser scanning microscopy. The cell nuclei were stained with DAPI (blue). (A) Fluolid-labeled polyplex micelles (orange) were distributed in tumor, liver, spleen and lymph nodes. (B) Intracellular uptake of Cy5-labeled pDNA (red) was depicted in tumor tissues. Scale bar = 100 (A) and 20 (B) μm.

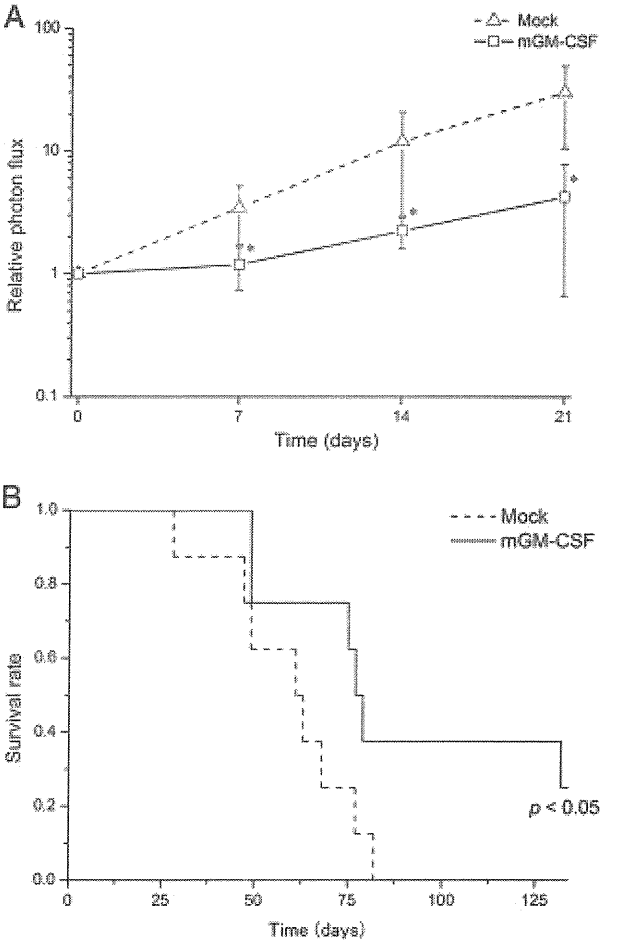

Fig. 3. Antitumor activity of block/homo polyplex micelles with mGM-CSF pDNA in nude mice with peritoneal dissemination. (A) Relative tumor volumes of SUIT-2/Luc peritoneal dissemination were analyzed with an IVIS imaging system in nude mice after i.p. administration of block/homo polyplex micelles with mock (△) or mGM-CSF (□) pDNA (50 μg pDNA/mouse). Results are represented as means ± SD (n = 5); *$p<0.05$ *versus* mock. (B) Kaplan–Meier survival curve for the nude mice bearing peritoneal dissemination after the treatment with block/homo polyplex micelles encapsulating mock or mGM-CSF pDNA (50 μg pDNA/mouse; n = 8).

micelle group on day 7 ($p<0.05$). On day 10 after injection, there was no significant difference between the two groups.

3.3. Tissue distribution of block/homo polyplex micelles

Upon higher luciferase expression with block/homo polyplex micelles, we examined the distribution locus of Fluolid-labeled block/homo polyplex micelles in tumor tissues and several normal organs (liver, spleen and lymph node) (Fig. 2A). The fluorescent signals of block/homo polyplex micelles were predominantly depicted at the stromal regions of tumor tissues. Furthermore, the fluorescent signals were also detected at the parenchymal regions in the liver, spleen and lymph nodes.

3.4. Intracellular uptake of pDNA into tumor tissues

Following the delivery of block/homo polyplex micelles to tissues, intracellular uptake is critical processes for transgene expression. Thus, we confirmed the intracellular uptake of Cy5-labeled pDNA in tumor tissues (Fig. 2B). Cy5 red-fluorescence was obviously observed in the cytoplasmic area of tumor cells dominantly with less signal in nuclei stained by DAPI.

3.5. Antitumor activity of block/homo polyplex micelles encapsulating mGM-CSF

The growth of disseminated pancreatic cancer was evaluated by bioluminescent signals from disseminated SUIT-2/Luc pancreatic cancer cells after i.p. administration of block/homo polyplex micelles with mGM-CSF or mock plasmid. As shown in Fig. 3A, the relative tumor volumes (V/V_0) were gradually increased in mock group (3.5 ± 1.7 on day 7; 11.9 ± 8.9 on day 14; 30.1 ± 19.6 on day 21). In contrast, the growth inhibition was obviously observed for mGM-CSF gene therapy (1.2 ± 0.5 on day 7; 2.2 ± 0.6 on day 14; 4.2 ± 3.6 on day 21). There were significant differences in tumor volume between the two groups on days 7, 14 and 21 ($p<0.05$).

We next compared the survival periods for mice harboring disseminated pancreatic cancer between mGM-CSF and mock groups. The median survival was significantly elongated with mGM-CSF gene therapy (78.0 ± 37.2 days) compared with the mock (62.0 ± 17.6 days). As

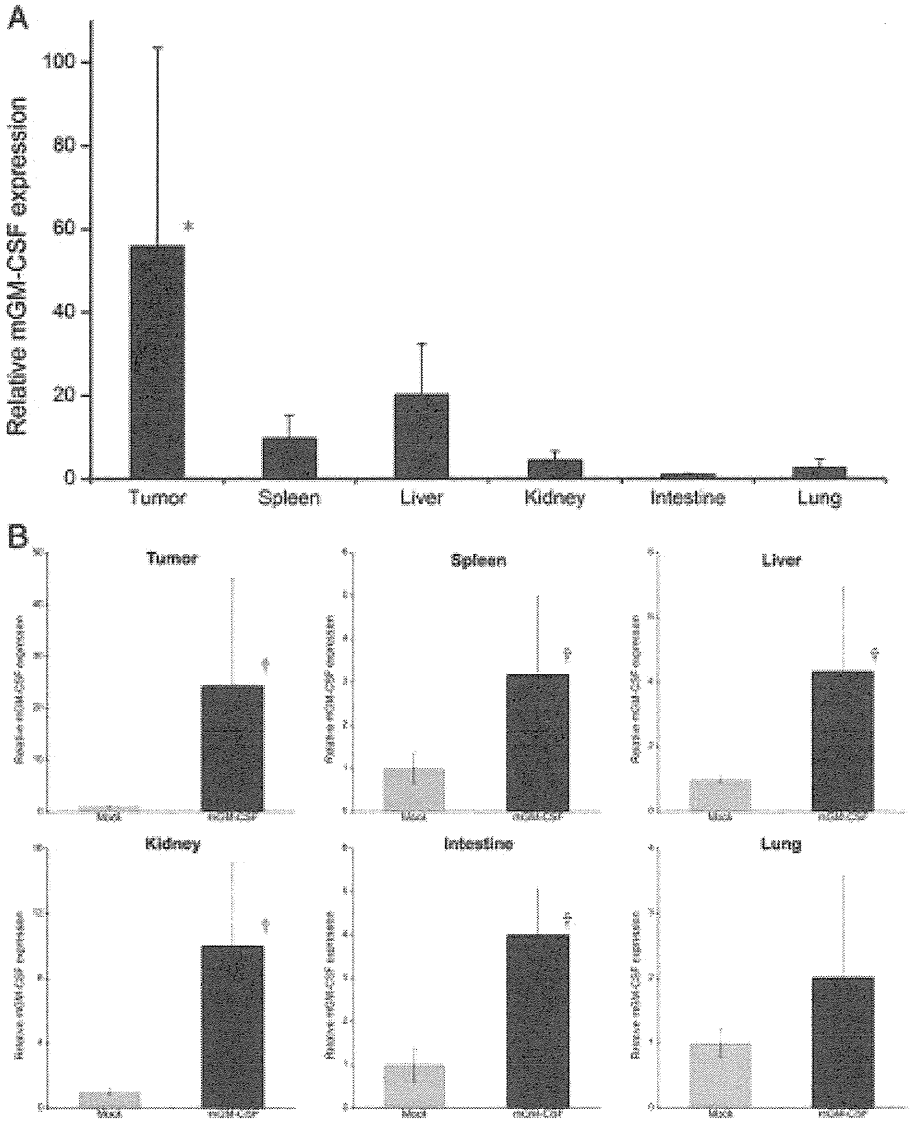

Fig. 4. qRT-PCR analysis for mGM-CSF mRNA expression in tumor and normal organ tissues. The indicated tissues were obtained from nude mice bearing SUIT-2/Luc peritoneal dissemination at 24 h after i.p. administration of block/homo polyplex micelles with mock or mGM-CSF pDNA (50 μg pDNA/mouse). Total RNA was extracted from tissue samples and subjected to qRT-PCR for mGM-CSF mRNA. (A) mGM-CSF mRNA expression was higher in tumors compared with normal organ tissues (*$p<0.05$). (B) mGM-CSF expression in the indicated tissues was upregulated by block/homo polyplex micelles with mGM-CSF pDNA compared with the mock (†$p<0.05$). Results are represented as means ± SD ($n=4$).

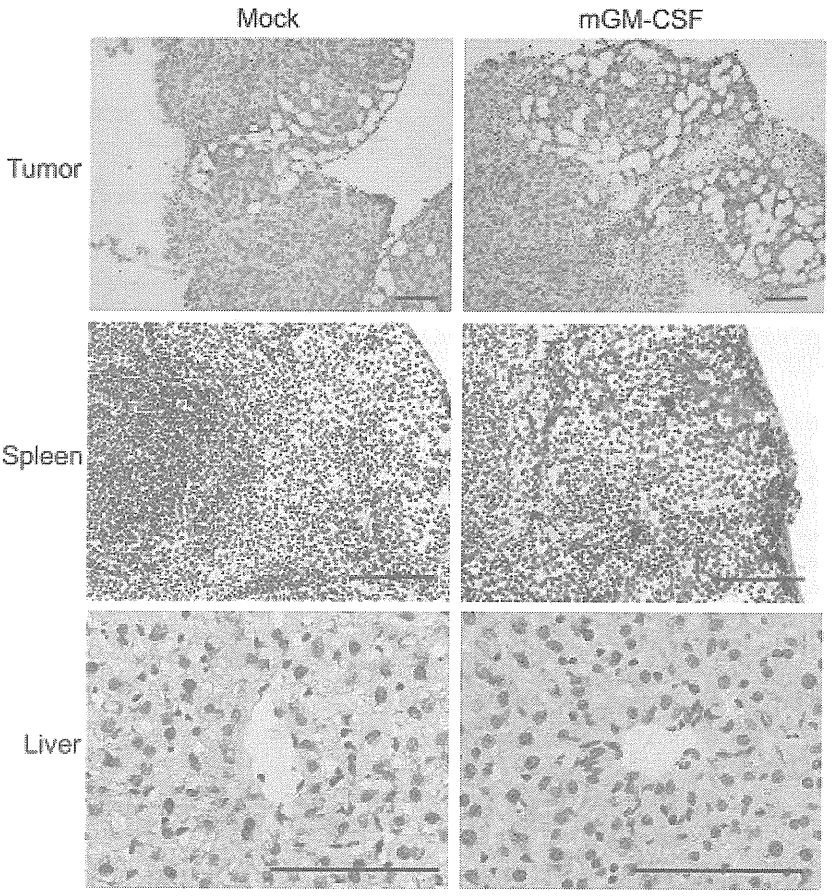

Fig. 5. Immunohistochemistry for mGM-CSF protein expression in tumor, spleen and liver tissues. The tissue samples were obtained from nude mice bearing SUIT-2/Luc peritoneal dissemination at 24 h after i.p. administration of block/homo polyplex micelles with mock or mGM-CSF pDNA (50 μg pDNA/mouse), and immunostained with an antibody for mouse GM-CSF. Scale bar = 100 μm.

shown in Kaplan–Meier survival curves (Fig. 3B), the survival rate was also higher in the mGM-CSF group than mock group ($p<0.05$).

3.6. Therapeutic gene expression in tumor and normal organ tissues

We examined the expression level and distribution of therapeutic gene: mGM-CSF by the qRT-PCR in tumor and various normal organ tissues on day 1 after i.p. administration of polyplex micelles (Fig. 4). Block/homo polyplex micelles with mGM-CSF induced 24-fold higher expression of mGM-CSF (24.3 ± 20.6) in tumor nodules compared with the mock group (1.00 ± 0.163; $p<0.05$, Fig. 4B). In normal organs of the spleen and liver, low level of mGM-CSF expression (9.70 ± 5.54; 20.2 ± 12.2, Fig. 4A) was detected. Similarly, the transgene expression of mGM-CSF was higher in the spleen (3.17 ± 1.81) and liver (4.31 ± 2.60) compared with the mock group. However, gene expression was fairly detected in other normal organs of kidney, lung, and intestine (4.43 ± 2.25; 2.63 ± 2.01; 1.00 ± 2.66, Fig. 4A). Thereafter, the mGM-CSF expression was gradually decreased in tumor and liver, whereas that in the spleen was once declined on day 2 but re-elevated on days 4 and 7, as shown in Supplementary Fig. 1.

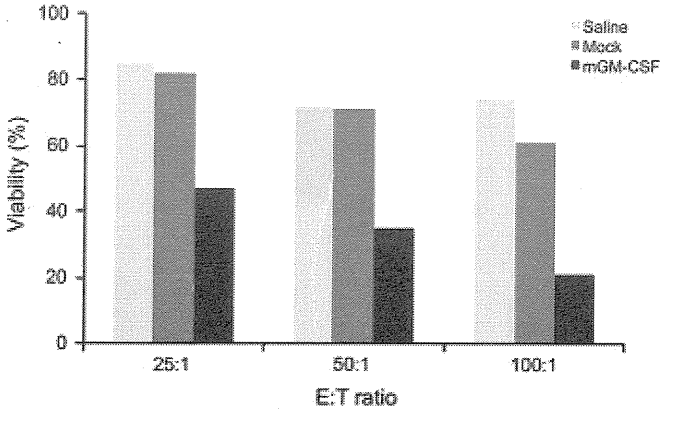

Fig. 6. Enhanced NK cytotoxicity by block/homo polyplex micelles with mGM-CSF pDNA. Splenocytes were isolated from nude mice with SUIT-2/Luc disseminated cancer on day 7 after i.p. administration of block/homo polyplex micelles encapsulating mock or mGM-CSF pDNA (50 μg pDNA/mouse), and co-incubated with CFSE-labeled YAC-1 cells. After 6 h incubation, the viability of YAC-1 was analyzed by flow cytometer. E:T ratio means the ratio of effector (splenocytes) to target cells (YAC-1). NK cytotoxicity assessed by the YAC-1 viability was enhanced by mGM-CSF gene therapy but not by saline or mock control.

The expression of mGM-CSF was confirmed in protein level by immunohistochemical analysis in tumor nodules, liver and spleen after administration of the block/homo polyplex micelles (Fig. 5). The mouse GM-CSF protein was detected in tumor tissues, and the localization was predominant in tumor stroma sites for mGM-CSF group. On the other hand, the expression of mGM-CSF was slightly observed in the spleen and liver for mGM-CSF group. In contrast, the expression of mGM-CSF was hardly detected in tumor, spleen and liver tissues for the mock group. The protein expression status in immunohistochemistry verified the data of mRNA expression in qRT-PCR, although it is difficult to discriminate transgene and endogenous GM-CSF expression.

3.7. Enhanced NK cytotoxicity by block/homo polyplex micelles with mGM-CSF

Because athymic nude mice lack T lymphocyte, we hypothesized that the antitumor effects of block/homo polyplex micelles loaded

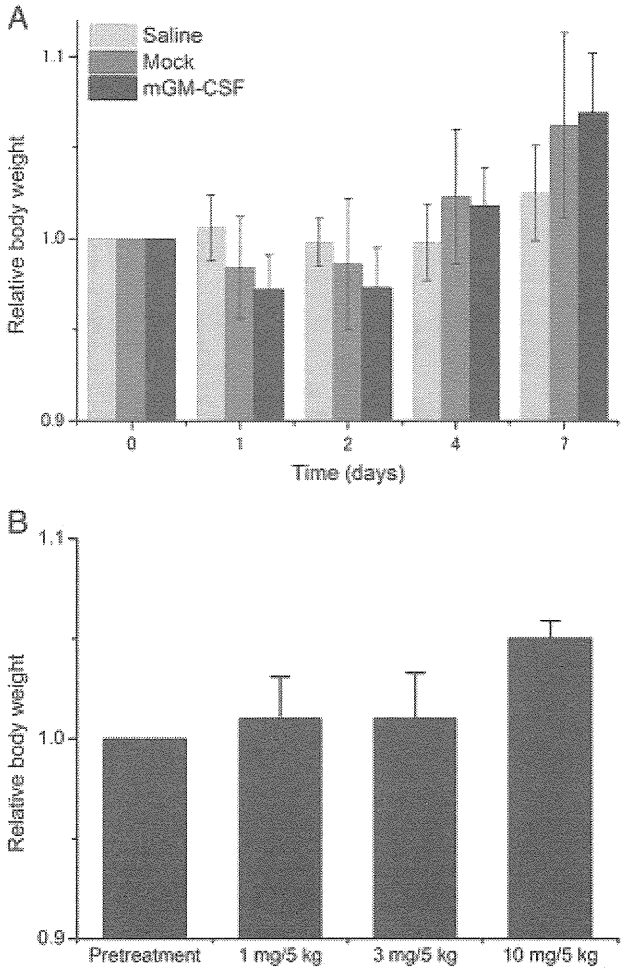

Fig. 7. Effect of i.p. administration of block/homo polyplex micelles on body weight in mice and cynomolgus monkeys. (A) Relative body weight changes in mice harboring SUIT-2/Luc peritoneal dissemination at the indicated time points after i.p. administration of block/homo polyplex micelles encapsulating mock or mGM-CSF pDNA (50 μg pDNA/mouse). (B) Relative body weight in cynomolgus monkeys at 24 h after i.p. administration of polyplex micelles with mock pDNA at the indicated dose. Results are represented as means ± SD (A, n = 8; B, n = 4).

with mGM-CSF might be attributed to enhancement in NK activity in tumor stroma and immune organs stimulated by GM-CSF. Flow cytometry showed that the number of CFSE-labeled viable target YAC-1 cells was decreased upon the higher ratio of effector: splenocytes to target cells for mGM-CSF gene therapy, but not changed for saline or mock group (Fig. 6). The NK activity, which was assessed by the viability of YAC-1 cells co-cultured with splenocytes, was significantly reduced in mGM-CSF group (47% in 25:1, 35% in 50:1, 21% in 100:1) compared with saline (85% in 25:1, 72% in 50:1, 74% in 100:1) and mock groups (72% in 25:1, 71% in 50:1, 61% in 100:1).

3.8. Toxicity study of block/homo polyplex micelles in mice model

Body weight was monitored as an indicator of overload influence for whole body. In mock and mGM-CSF group, relative body weight was slightly reduced on days 1 and 2 and thereafter returned to the same level as saline group. There were no significant differences between the groups (Fig. 7A).

Table 1 summarizes the results in blood hematology tests. There were no significant differences in WBC, RBC, HCT and PLT between normal and mGM-CSF group, except for the WBC and PLT at 24 h. In mGM-CSF group, WBC and PLT values were slightly decreased at 24 h (31.0 ± 5.0 and 46.7 ± 9.8, respectively) compared with those of normal group (42.2 ± 4.7 and 75.4 ± 6.5, respectively), despite the decreased values were within normal range and returned to basal level at 72 h. Blood chemistry tests for mice treated i.p. with saline, mock and mGM-CSF block/homo polyplex micelles are shown in Table 1. The renal function assessed by creatinine concentration was not impaired in saline, mock and mGM-CSF gene therapy groups. The hepatic function evaluated by ALT, AST and total bilirubin concentrations was not disturbed in all three groups, although the ALT value at 24 h was slightly lower in mGM-CSF group. The LDH concentrations as an index of cell membrane damage also did not change, and no significance was observed between normal and mGM-CSF groups.

3.9. Toxicity study of block/homo polyplex micelles in cynomolgus monkey

Physical findings: there were no decedents or moribund behavior during 7 days after i.p. administration of each dose of block/homo polyplex micelles. Furthermore, no other aberrant findings in behavior, status of visible mucous membrane, food consumption and character of

Table 1
Hematology and blood chemistry tests for BALB/c mice at 24 and 72 h after intraperitoneal administration of polyplex micelles encapsulating pDNA.

Hematology tests		WBC (10^2/μL)	RBC (10^4/μL)	HCT (%)	PLT (10^4/μL)
Normal	–	42.2 ± 4.7	976 ± 79	49.9 ± 4.2	75.4 ± 6.5
Saline	24 h	40.0 ± 12	894 ± 87	46.0 ± 5.0	104 ± 3.4*
	72 h	39.7 ± 9.3	929 ± 51	47.0 ± 2.8	70.8 ± 15
Mock	24 h	28.4 ± 4.2*	883 ± 73	45.4 ± 4.3	78.0 ± 18
	72 h	39.0 ± 20	944 ± 29	48.0 ± 1.4	93.4 ± 6.7*
mGM-CSF	24 h	31.0 ± 5.0*	945 ± 96	49.4 ± 5.2	46.7 ± 9.8*
	72 h	41.0 ± 4.5	919 ± 30	47.4 ± 1.7	71.9 ± 7.8

Blood chemistry tests		Creatinine (mg/dL)	ALT (IU/L)	AST (IU/L)	Total bilirubin (mg/dL)	LDH (IU/L)
Normal	–	0.21 ± 0.07	31 ± 4	54 ± 10	0.04 ± 0.02	206 ± 67
Saline	24 h	0.13 ± 0.01*	35 ± 5	62 ± 14	0.04 ± 0.01	197 ± 27
	72 h	0.15 ± 0.03	30 ± 4	53 ± 8	0.05 ± 0.01	175 ± 32
Mock	24 h	0.16 ± 0.02	30 ± 4	54 ± 5	0.04 ± 0.01	208 ± 74
	72 h	0.15 ± 0.04	27 ± 2	51 ± 10	0.05 ± 0.01	235 ± 50
mGM-CSF	24 h	0.16 ± 0.02	26 ± 3*	57 ± 14	0.03 ± 0.01	216 ± 63
	72 h	0.16 ± 0.03	29 ± 4	48 ± 8	0.03 ± 0.01	183 ± 31

WBC, white blood cell; RBC, red blood cell; HCT, hematocrit; PLT, platelet; ALT, alanine aminotransferase; AST, aspartate aminotransferase; LDH, lactate dehydrogenase.
Results are represented as means ± SD (n = 5).
* $p < 0.05$ *versus* normal.

Table 2
Effect of intraperitoneal administration of block/homo polyplex micelles on physical and pathological findings in cynomolgus monkeys.

	Evaluations	Effect of polyplex micelles
Clinical symptoms	Body weight change Food consumption	No effect
Gross pathology	Adrenal gland, aorta, cecum, cerebellum, cerebrum, colon, duodenum, epididymides, esophagus, eye, femur skeletal muscle, femur, gallbladder, heart, ileum, jejunum, kidney, liver, lung, mammary gland, medulla oblongata, mesenteric lymph node, optic nerve, ovary, pancreas, parotid gland, pharynx, pituitary gland, prostate, rectum, sciatic nerves, seminal vesicle, skin, spinal cord, spleen, sternum, stomach, sublingual gland, submandibular gland, submandibular lymph node, testes, thymus, thyroid, tongue, trachea, urinary bladder, uterus, vagina and gross lesions	No effect
Organ weights and organ to body weight ratios	Adrenal gland, brain, bladder, heart, kidney, liver, lung, pancreas, pituitary gland, prostate, seminal vesicle/uterus, spleen, submandibular gland, testes/ovaries, thymus and thyroid	No effect

feces were observed (Table 2). Body weight was not affected by block/homo polyplex micelle treatment in all doses (Fig. 7B).

Pathological findings: No gross abnormalities in any organs were observed at the scheduled autopsy (Table 2).

Blood examinations: hematological and blood chemistry parameters are summarized in Table 3. The increase of fibrinogen was observed at the next day of block/homo polyplex micelle injection in monkeys with all dose groups; however, prothrombin time and activated partial thrombin time were not affected. Changes in lymphocyte, neutrophil, AST and LDH were observed in some cases, but the values were kept within the limits of accidental variation (Table 3).

4. Discussion

Efficient gene transduction and high safety potentials *in vivo* are most important determinants to apply gene therapy in clinical settings. We have demonstrated the accumulation and gene transduction of block/homo polyplex micelles in tumor tissues by i.p. administration. The distribution of micelles into normal organs of the liver, spleen and lymph node was also observed. The resultant gene expression in tumor and immune organs rendered to the antitumor efficacy of GM-CSF gene therapy *via* enhanced NK activity in nude mice with refractory disseminated pancreatic cancer. We have also validated high capacities of safety reserve for i.p. administration of block/homo polymer micelles not only in mice but also in cynomolgus monkeys, implicating the potential of block/homo-mixed polyplex-based gene therapy for clinical application.

The luciferase transgene expression *in vivo* showed much higher by i.p. administration of block/homo polyplex micelles compared with that of block polyplex micelles (Fig. 1). To examine the location of block/homo polyplex micelles, we performed the distribution study using Fluolid-labeled polyplex micelles. The accumulation of the labeled polyplex was detected in tumor nodules, because the block/homo polyplex micelles were around 100 nm in size and influenced by EPR effect [24] after adsorbed into peritoneal vessels, as demonstrated in the distribution study for i.p. administered gold nanoparticles [25], in addition to the direct penetration into the tumors without surface coverage. Furthermore, the localization of Fluolid-labeled micelles in tumor tissues was dominant at the stromal region (Fig. 2A). In tumor tissues, high interstitial pressure within tumor nests and severe fibrosis around tumor nests are obstacles for drug penetration [26–28]. Because over 50 nm micelles are not able to penetrate into the deep area in tumor nests of pancreatic cancer [29], block/homo polyplex micelles (90.2 ± 2.05 nm) were localized only in the stromal region. Moreover, Cy5-labeled pDNA was clearly uptaken into the cytoplasmic area of cells in tumor nodules for block/homo polyplex micelles (Fig. 2B). These results indicate that i.p. administration of block/homo polyplex micelles has high potential of transfection activity, as well as other administration methods [16,17]. Distribution and transgene expression in normal organs, such as the liver, spleen and lymph nodes, were also elicited by i.p. administration of block/homo polyplex micelles (Figs. 2A, 4). There are mainly two delivery routes of polyplex micelles *via* portal and lymphatic vessels after i.p. injection, except the direct penetration into tumor tissues without coverage of serosal membranes. The polyplex micelles after i.p. injection may be absorbed into the portal and lymphatic vessel, and were distributed in the parenchymal regions of the liver, spleen and lymph node. Accordingly, transgene expression was observed not only in tumor but also in these immune organs (Fig. 4).

Carrier distribution and transgene expression in tumor stroma and immune organs exhibit preferable performance when block/homo polyplex micelles are applied for immunogene therapy. We thus use the i.p. administered block/homo polyplex micelles as a carrier of GM-CSF immunogene and examined the antitumor efficacy. Prior to the assessment *in vivo*, we confirmed no direct cytotoxicity

Table 3
Effect of intraperitoneal administration of block/homo polyplex micelles on parameters for hematology, blood chemistry and coagulation tests in cynomolgus monkeys.

	Evaluations	Effect of polyplex micelles
Hematology	White blood cells, red blood cells, hemoglobin, hematocrit, mean corpuscular volume, mean corpuscular hemoglobin, mean corpuscular hemoglobin concentration, platelets, neutrophils, lymphocytes, monocytes, eosinophils and basophils	No effect
Blood chemistry	Albumin, alkaline phosphatase, alanine aminotransferase, aspartate aminotransferase, blood urea nitrogen, calcium, cholesterol, chloride, creatinine, glucose, phospholipid, potassium, sodium, phosphorus, total bilirubin, total protein and triglycerides	No effect
Blood coagulation	Prothrombin time and activated partial thrombin time Fibrinogen	No effect *Elevation* Male: 272 ± 4.9 (pre) → 448 ± 28 (1 mg/5 kg), 553 ± 74 (5 mg/5 kg) and 680 ± 14 mg/dL (10 mg/5 kg) Female: 330 ± 66 (pre) → 507 ± 2.8 (1 mg/5 kg), 501 ± 51 (5 mg/5 kg) and 780 ± 140 mg/dL (10 mg/5 kg)

Results are represented as means ± SD (n = 2 in each male and female).

of mGM-CSF for human SUIT-2 cancer cells *in vitro* (data not shown). *In vivo* tumor growth assay revealed that the mGM-CSF gene therapy with block/homo polyplex micelles induced a significant tumor growth inhibition and prolonged the survival for mice bearing pancreatic SUIT-2 disseminated cancer (Fig. 3). In qRT-PCR and immunohistochemical analyses, block/homo polyplex micelles transduced higher level of mGM-CSF mRNA and protein expression in tumor tissues (Figs. 4, 5). In the spleen and liver among normal organs, mGM-CSF expression was detected to less extent (Figs. 4A, 5). It is well known that GM-CSF, an immunostimulatory cytokine produced by monocyte, mast cell, endothelial cell and other immune cells [30,31], induces tumoricidal activity through the activation of dendritic cell, macrophage, natural killer (NK) cells and lymphocytes [31–33]. In particular, NK cells play a key role for killing tumor cells in nude mice bearing tumor [34]. In this study, NK activity of splenocytes was strongly enhanced by i.p. administration of block/homo polyplex micelles loaded with mGM-CSF pDNA but not with mock (Fig. 6). The mGM-CSF expression in tumor and liver was maximally elevated on day 1 and then decreased gradually, whereas that in the spleen was once declined but re-elevated on days 4 and 7 (Supplementary Fig. 1). The NK activation may be induced not only by transduced mGM-CSF in tumor stroma but also by endogenous mGM-CSF up-regulation in the spleen due to the secondary immune-response, because transgene (luciferase) expression was decreased in a time-dependent manner (Fig. 1). These results demonstrate that i.p. administration of block/homo polyplex micelles with the immunogene may induce the antitumor activity due to the immunostimulatory effects in immune organs and tumor stromas. Regarding the administration site, i.p. administration of polyplex micelles could keep high concentration of mGM-CSF in peritoneal tumors, although mGM-CSF is secreted to the distant tumor sites after s.c. administration. In addition, the transduced mGM-CSF gene in the spleen might induce strong antitumor effect, because the spleen is a central organ for systemic immunity. Thus, we designed i.p. administration of polyplex micelles for mice with peritoneal dissemination in this study. However, s.c. administration of polyplex micelles has advantages in clinical application, and the comparative study for administration sites should be addressed to several tumor models in future.

Block/homo polyplex micelles achieved the sufficient level of transgene expression to inhibit peritoneal dissemination of pancreatic cancer; however some concerns regarding the biocompatibility *in vivo* are remained due to the decrease of PEGylation density compared to the polyplex micelles composed only with PEG-*b*-P[Asp(DET)] block copolymer. Therefore, we evaluated the toxicity of block/homo polyplex micelles in mouse and monkey models. In mice experiments, body weight was slightly reduced just after i.p. administration of polyplex micelles (Fig. 7A), which is consistent with a previous report for PEG-ss-P[Asp(DET)] [15]. The transient body weight loss in mice might be due to the decreased intake of food and water by peritoneal irritation and anesthesia, because no change in body weight was observed in large animal model of cynomolgus monkeys (Fig. 7B). There were no significant abnormalities in almost hematological parameters for mGM-CSF group except the transient decrease at 24 h of WBC and PLT (Table 1), yet the reduced WBC and PLT values were within a normal range in clinical evaluation. Regarding renal and hepatic functions, no significant injury was induced in mice disease model of peritoneal dissemination by mGM-CSF gene therapy (Table 1). In monkey models, there were no significant abnormal changes in hematology and blood chemistry tests (Table 3). In blood coagulation tests, fibrinogen concentration was increased in monkeys by i.p. administration of polyplex micelles, although the reason was not identified. However, prothrombin time and activated partial thrombin time were not affected, suggesting that the increased fibrinogen might not indicate serious coagulopathy, such as disseminated intravascular coagulation (DIC). Furthermore, other findings at autopsy, such as gross pathology and relative organ weight, did not show any injury in whole organs (Table 2). These results strongly suggest that block/homo mixed polyplex micelle is a gene carrier with high safety capacity when applied *via* i.p. administration.

In conclusion, the antitumor immunity elicited by GM-CSF gene transduction in tumor and immune organs, such as the liver, spleen and lymph nodes, and high safety potential of i.p. administered block/homo polyplex micelles are demonstrated in mice with peritoneal dissemination and healthy cynomolgus monkeys. Block/homo polyplex-based immunogene therapy could open a way to clinical application of gene therapy for refractory disseminated cancer.

Supplementary data to this article can be found online at http://dx.doi.org/10.1016/j.jconrel.2013.02.006.

Acknowledgments

This work was financially supported in part by the Grants-in-Aid for Scientific Research to K.N. from the Japanese Ministry of Education, Culture, Sports, Science and Technology, Japan (MEXT) (project code: 24390322) and the Special Coordination Funds for Promoting Science and Technology (SCF funding program Grants-in-Aid for Scientific Research from Japan). This research is also partly supported by the Core Research Program for Evolutional Science and Technology (CREST) to K.K. from Japan Science and Technology Agency (JST). We appreciate Drs. Nobuhiro Nishiyama, Kensuke Osada and Takehiko Ishii (The University of Tokyo) for helpful discussion, and Drs. Takaaki Kanemaru, Michiaki Kumagai, Shinya Shimoda and Mrs. Aya Sakai (Kyushu University) for technical assistance.

References

[1] M.A. Kay, State-of-the-art gene-based therapies: the road ahead, Nat. Rev. Genet. 12 (2011) 316–328.
[2] F. Mingozzi, K.A. High, Therapeutic in vivo gene transfer for genetic disease using AAV: progress and challenges, Nat. Rev. Genet. 12 (2011) 341–355.
[3] N.B. Wasala, J.H. Shin, D.S. Duan, The evolution of heart gene delivery vectors, J. Gene Med. 13 (2011) 557–565.
[4] C. Scholz, E. Wagner, Therapeutic plasmid DNA versus siRNA delivery: common and different tasks for synthetic carriers, J. Control. Release 161 (2012) 554–565.
[5] M. Morille, C. Passirani, A. Vonarbourg, A. Clavreul, J.P. Benoit, Progress in developing cationic vectors for non-viral systemic gene therapy against cancer, Biomaterials 29 (2008) 3477–3496.
[6] M. Elsabahy, A. Nazarali, M. Foldvari, Non-viral nucleic acid delivery: key challenges and future directions, Curr. Drug Deliv. 8 (2011) 235–244.
[7] K. Miyata, M. Oba, M. Nakanishi, S. Fukushima, Y. Yamasaki, H. Koyama, N. Nishiyama, K. Kataoka, Polyplexes from poly(aspartamide) bearing 1,2-diaminoethane side chains induce pH-selective, endosomal membrane destabilization with amplified transfection and negligible cytotoxicity, J. Am. Chem. Soc. 130 (2008) 16287–16294.
[8] K. Itaka, T. Ishii, Y. Hasegawa, K. Kataoka, Biodegradable polyamino acid-based polycations as safe and effective gene carrier minimizing cumulative toxicity, Biomaterials 31 (2010) 3707–3714.
[9] H.J. Kim, A. Ishii, K. Miyata, Y. Lee, S.R. Wu, M. Oba, N. Nishiyama, K. Kataoka, Introduction of stearoyl moieties into a biocompatible cationic polyaspartamide derivative, PAsp(DET), with endosomal escaping function for enhanced siRNA-mediated gene knockdown, J. Control. Release 145 (2010) 141–148.
[10] N. Kanayama, S. Fukushima, N. Nishiyama, K. Itaka, W.D. Jang, K. Miyata, Y. Yamasaki, U.I. Chung, K. Kataoka, A PEG-based biocompatible block catiomer with high buffering capacity for the construction of polyplex micelles showing efficient gene transfer toward primary cells, ChemMedChem 1 (2006) 439–444.
[11] K. Itaka, S. Ohba, K. Miyata, H. Kawaguchi, K. Nakamura, T. Takato, U.I. Chung, K. Kataoka, Bone regeneration by regulated in vivo gene transfer using biocompatible polyplex nanomicelles, Mol. Ther. 15 (2007) 1655–1662.
[12] M. Harada-Shiba, I. Takamisawa, K. Miyata, T. Ishii, N. Nishiyama, K. Itaka, K. Kangawa, F. Yoshihara, Y. Asada, K. Hatakeyama, N. Nagaya, K. Kataoka, Intratracheal gene transfer of adrenomedullin using polyplex nanomicelles attenuates monocrotaline-induced pulmonary hypertension in rats, Mol. Ther. 17 (2009) 1180–1186.
[13] T. Nomoto, Y. Matsumoto, K. Miyata, M. Oba, S. Fukushima, N. Nishiyama, T. Yamasoba, K. Kataoka, In situ quantitative monitoring of polyplexes and polyplex micelles in the blood circulation using intravital real-time confocal laser scanning microscopy, J. Control. Release 151 (2011) 104–109.
[14] S. Takae, K. Miyata, M. Oba, T. Ishii, N. Nishiyama, K. Itaka, Y. Yamasaki, H. Koyama, K. Kataoka, PEG-detachable polyplex micelles based on disulfide-linked block catiomers as bioresponsive nonviral gene vectors, J. Am. Chem. Soc. 130 (2008) 6001–6009.
[15] M. Kumagai, S. Shimoda, R. Wakabayashi, Y. Kunisawa, T. Ishii, K. Osada, K. Itaka, N. Nishiyama, K. Kataoka, K. Nakano, Effective transgene expression without toxicity by intraperitoneal administration of PEG-detachable polyplex micelles in mice with peritoneal dissemination, J. Control. Release 160 (2012) 542–551.

[16] Q.X. Chen, K. Osada, T. Ishii, M. Oba, S. Uchida, T.A. Tockary, T. Endo, Z.S. Ge, H. Kinoh, M.R. Kano, K. Itaka, K. Kataoka, Homo-catiomer integration into PEGylated polyplex micelle from block-catiomer for systemic anti-angiogenic gene therapy for fibrotic pancreatic tumors, Biomaterials 33 (2012) 4722–4730.
[17] S. Uchida, K. Itaka, Q.X. Chen, K. Osada, T. Ishii, M.A. Shibata, M. Harada-Shiba, K. Kataoka, PEGylated polyplex with optimized peg shielding enhances gene introduction in lungs by minimizing inflammatory responses, Mol. Ther. 20 (2012) 1196–1203.
[18] P. Jacquet, P.H. Sugarbaker, Peritoneal–plasma barrier, Cancer Treat. Res. 82 (1996) 53–63.
[19] Z. Lu, J. Wang, M.G. Wientjes, J.L.S. Au, Intraperitoneal therapy for peritoneal cancer, Future Oncol. 6 (2010) 1625–1641.
[20] M. Markman, Intraperitoneal drug delivery of antineoplastics, Drugs 61 (2001) 1057–1065.
[21] T. Kamei, J. Kitayama, H. Yamaguchi, D. Soma, S. Emoto, T. Konno, K. Ishihara, H. Ishigami, S. Kaisaki, H. Nagawa, Spatial distribution of intraperitoneally administrated paclitaxel nanoparticles solubilized with poly (2-methacryloxyethyl phosphorylcholine-co n-butyl methacrylate) in peritoneal metastatic nodules, Cancer Sci. 102 (2011) 200–205.
[22] M. Mitsui, M. Nishikawa, L. Zang, M. Ando, K. Hattori, Y. Takahashi, Y. Watanabe, Y. Takakura, Effect of the content of unmethylated CpG dinucleotides in plasmid DNA on the sustainability of transgene expression, J. Gene Med. 11 (2009) 435–443.
[23] I. Jedema, N.M. van der Werff, R.M.Y. Barge, R. Willemze, J.H.F. Falkenburg, New CFSE-based assay to determine susceptibility to lysis by cytotoxic T cells of leukemic precursor cells within a heterogeneous target cell population, Blood 103 (2004) 2677–2682.
[24] Y. Matsumura, H. Maeda, A new concept for macromolecular therapeutics in cancer-chemotherapy — mechanism of tumoritropic accumulation of proteins and the antitumor agent Smancs, Cancer Res. 46 (1986) 6387–6392.
[25] R.R. Arvizo, O.R. Miranda, D.F. Moyano, C.A. Walden, K. Giri, R. Bhattacharya, J.D. Robertson, V.M. Rotello, J.M. Reid, P. Mukherjee, Modulating pharmacokinetics, tumor uptake and biodistribution by engineered nanoparticles, PLoS One 6 (2011) 1–6.
[26] A.I. Minchinton, I.F. Tannock, Drug penetration in solid tumours, Nat. Rev. Cancer 6 (2006) 583–592.
[27] M. Yashiro, Y.S. Chung, S. Nishimura, T. Inoue, M. Sowa, Fibrosis in the peritoneum induced by scirrhous gastric cancer cells may act as "soil" for peritoneal dissemination, Cancer 77 (1996) 1668–1675.
[28] R.K. Jain, Barriers to drug-delivery in solid tumors, Sci. Am. 271 (1994) 58–65.
[29] H. Cabral, Y. Matsumoto, K. Mizuno, Q. Chen, M. Murakami, M. Kimura, Y. Terada, M.R. Kano, K. Miyazono, M. Uesaka, N. Nishiyama, K. Kataoka, Accumulation of sub-100 nm polymeric micelles in poorly permeable tumours depends on size, Nat. Nanotechnol. 6 (2011) 815–823.
[30] N.M. Gough, J. Gough, D. Metcalf, A. Kelso, D. Grail, N.A. Nicola, A.W. Burgess, A.R. Dunn, Molecular-cloning of cDNA-encoding a murine hematopoietic growth-regulator, granulocyte macrophage colony stimulating factor, Nature 309 (1984) 763–767.
[31] M. Jinushi, H. Tahara, Cytokine gene-mediated immunotherapy: current status and future perspectives, Cancer Sci. 100 (2009) 1389–1396.
[32] L. de la Cruz-Merino, E. Grande-Pulido, A. Albero-Tamarit, M.E.C.M. de Villena, Cancer and immune response: old and new evidence for future challenges, Oncologist 13 (2008) 1246–1254.
[33] P.E. Tarr, Granulocyte-macrophage colony-stimulating factor and the immune system, Med. Oncol. 13 (1996) 133–140.
[34] J. Dou, Y.F. Wang, J. Wang, F.S. Zhao, Y.T. Li, M.G. Cao, W.H. Hu, K. Hu, X.F. He, L.L. Chu, C.L. Jiang, N. Gu, Antitumor efficacy induced by human ovarian cancer cells secreting IL-21 alone or combination with GM-CSF cytokines in nude mice model, Immunobiology 214 (2009) 483–492.

Biomaterials 34 (2013) 562–570

Contents lists available at SciVerse ScienceDirect

Biomaterials

journal homepage: www.elsevier.com/locate/biomaterials

Silica nanogelling of environment-responsive PEGylated polyplexes for enhanced stability and intracellular delivery of siRNA

Noha Gouda [a,b], Kanjiro Miyata [c,**], R. James Christie [c], Tomoya Suma [a], Akihiro Kishimura [d], Shigeto Fukushima [d], Takahiro Nomoto [a], Xueying Liu [c], Nobuhiro Nishiyama [c], Kazunori Kataoka [a,c,d,e,*]

[a] Department of Bioengineering, Graduate School of Engineering, The University of Tokyo, 7-3-1 Hongo, Bunkyo-ku, Tokyo 113-8656, Japan
[b] Department of Pharmaceutics, Faculty of Pharmacy, Alexandria University, Azarita, Khartoum square, Alexandria 21521, Egypt
[c] Center for Disease Biology and Integrative Medicine, Graduate School of Medicine, The University of Tokyo, 7-3-1 Hongo, Bunkyo-ku, Tokyo 113-0033, Japan
[d] Department of Materials Engineering, Graduate School of Engineering, The University of Tokyo, 7-3-1 Hongo, Bunkyo-ku, Tokyo 113-8656, Japan
[e] Center for NanoBio Integration, The University of Tokyo, 7-3-1 Hongo, Bunkyo-ku, Tokyo 113-8656, Japan

ARTICLE INFO

Article history:
Received 16 August 2012
Accepted 29 September 2012
Available online 17 October 2012

Keywords:
siRNA delivery
Polyplex
Silica
PEG
Disulfide cross-link

ABSTRACT

In this study, poly(ethylene glycol) (PEG)-block-polycation/siRNA complexes (PEGylated polyplexes) were wrapped with a hydrated silica, termed "silica nanogelling", in order to enhance their stability and functionality. Silica nanogelling was achieved by polycondensation of soluble silicates onto the surface of PEGylated polyplexes comprising a disulfide cross-linked core. Formation of silica nanogel layer on the PEGylated cross-linked polyplexes was confirmed by particle size increase, surface charge reduction, and elemental analysis of transmission electron micrographs. Silica nanogelling substantially improved polyplex stability against counter polyanion-induced dissociation under non-reductive condition, without compromising the reductive environment-responsive siRNA release triggered by disulfide cleavage. Silica nanogelling significantly enhanced the sequence-specific gene silencing activity of the polyplexes in HeLa cells without associated cytotoxicity, probably due lower endosomal entrapment (or lysosomal degradation) of delivered siRNA. The lower endosomal entrapment of the silica nanogel system could be explained by an accelerated endosomal escape triggered by deprotonated silanol groups in the silica (the proton sponge hypothesis) and/or a modulated intracellular trafficking, possibly *via* macropinocytosis, as evidenced by the cellular uptake inhibition assay. Henceforth, silica nanogelling of PEGylated siRNA polyplexes is a promising strategy for preparation of stable and functional siRNA delivery vehicles.

1. Introduction

Small interfering RNA (siRNA) has opened wide new horizons for therapeutic mechanisms for a variety of intractable diseases [1–3], as it can induce potent sequence-specific gene silencing, termed RNA interference (RNAi) [4]. However, when administered in the body, siRNA is susceptible to degradation by serum nucleases and to rapid elimination *via* the kidneys. These inherent drawbacks of siRNA substantially compromise its *in vivo* gene silencing activity, hence necessitating the use of carrier systems for its successful delivery to the cytoplasm of target cell. Examples of the types of carrier systems that have been developed for siRNA delivery include: cationic lipid-based complexes (lipoplexes) [5–8], polycation-based complexes (polyplexes) [9–17], inorganic nanoparticles [18–20], and their hybrid systems [21–24]. Nevertheless, there is still a great need for more efficient and safer carrier formulations for clinical application of siRNA therapeutics.

One promising approach for development of siRNA carriers is to construct environment-responsive nanoparticles that stably enclose siRNA while in extracellular conditions protecting it from enzymatic degradation and renal clearance, whereas releasing siRNA in the cytoplasm of target cells to induce RNAi. For this purpose, intracellularly cleavable linkers, such as the disulfide bond, have been integrated into carrier components to provide polyplexes with the reversible stability in response to cytoplasmic reducing potential [25]. Previous studies have reported the cross-linking of poly(ethylene glycol)-modified (PEGylated) polyplexes by environment-

* Corresponding author. Department of Bioengineering, Graduate School of Engineering, The University of Tokyo, 7-3-1 Hongo, Bunkyo-ku, Tokyo 113-8656, Japan. Tel.: +81 3 5841 7138; fax: +81 3 5841 7139.
** Corresponding author. Tel.: +81 3 5841 1701; fax: +81 3 5841 7139.
E-mail addresses: miyata@bmw.t.u-tokyo.ac.jp (K. Miyata), kataoka@bmw.t.u-tokyo.ac.jp (K. Kataoka).

0142-9612/$ – see front matter © 2012 Elsevier Ltd. All rights reserved.
http://dx.doi.org/10.1016/j.biomaterials.2012.09.077

responsive disulfide bonds for enhanced stability and biocompatibility in extracellular non-reductive conditions [26–29]. The obtained PEGylated cross-linked polyplexes (PCPs) successfully improved the gene silencing activity in cultured cells. Nevertheless, the PCPs apparently require further stabilization for the longevity in the bloodstream, as their blood half-life was still less than 15 min, although it was significantly longer than naked siRNA [28].

A major mechanism for polyplex destabilization/dissociation in the body is counter polyanion exchange reaction between polyplexes and negatively charged biomacromolecules, such as albumin and heparan sulfate. These biomacromolecules can directly bind to the polyplex-forming polycations to form ion pairs, resulting in release of free siRNA. Non-ionic, hydrophilic, and highly flexible PEG shielding is one of the approaches commonly used to reduce non-specific interactions of polyplexes with biomacromolecules [30–32], however additional surface shielding is still needed for complete inhibition of those undesired interactions. In this regard, we focused on silica nanogel shielding of polyplexes using soluble silicates; the silica nanogel layer can be formed directly on the polyplex surface through condensation of anionic silicic acid species in the vicinity of polycations [33–36] to form a gel layer sufficiently covering the net positive charge of polyplexes (Fig. 1). The resulting silica gel layer can be gradually degraded in dilute conditions into small silicate species [37], which are readily excreted *via* the kidneys [38]. Indeed, our recent study demonstrated that the anionic silica layer was successfully prepared on non-PEGylated siRNA polyplex surface, transiently stabilizing the polyplex structure and allowing additional surface modification with polycationic materials by a layer-by-layer technique toward multifunctional siRNA delivery [36].

In the present study, the silica nanogelling was utilized to wrap the siRNA PCPs equipped with PEG palisade in order to improve their stability and functionality. The outer silica nanogel layer provided a negatively charged protective shell surrounding the PCPs minimizing their vulnerability against the polyanion-induced dissociation under non-reductive conditions. Meanwhile, the disulfide cleavage in the polyplex core compromised the protective effect of silica nanogelling, leading to the selective release of the siRNA payload under reductive conditions, such as the cytoplasm. The formation of a silica nanogel layer on the PCP surface was verified from the change in size and surface charge, as well as from elemental mapping by energy dispersive X-ray (EDX) analysis measured by scanning transmission electron microscopy (STEM). Furthermore, effect of reversible stability of polyplexes was examined on siRNA release under non-reductive and reductive environments. The biological effect of the silica nanogel wrapping on gene silencing activity in cultured cancer cells, and also the effect on transfection mechanisms, including cellular uptake, endocytic pathway, and intracellular trafficking, were investigated. Ultimately, it was demonstrated that the silica nanogelling is a promising approach for reversible stabilization and functionalization of PCPs toward enhanced siRNA delivery.

2. Materials and methods

2.1. Materials

Firefly GL3 luciferase siRNA (siGL3) (sense: 5′-CUU ACG CUG AGU ACU UCG AdTdT-3′; antisense: 5′-UCGAAG UAC UCA GCG UAA GdTdT-3′), Cy5-labeled siGL3 (Cy5-siGL3), and scramble siRNA (siSCR) (sense: 5′-UUC UCC GAA CGU GUC ACG UdTdT-3′; antisense: 5′-ACG UGA CAG GUU CGG AGA AdTdT-3′) were synthesized by Hokkaido System Science Co., Ltd. (Hokkaido, Japan). The block copolymer, poly(ethylene glycol)-*block*-poly(L-lysine) (PEG-PLL) was synthesized as previously described [39]. Sodium silicate solution reagent grade (~27% SiO_2), Dulbecco's modified Eagle's medium (DMEM), trypsine-ethylenediaminetetraacetate (EDTA) solution (10×), Amiloride hydrochloride hydrate, dithiothreitol (DTT), and chlorpromazine hydrochloride were purchased from Sigma Aldrich Co. (St. Louis, MO, USA). Dimethyl sulfoxide (DMSO) was purchased from Tokyo Chemical Industry Co. Ltd. (Tokyo, Japan). Sterile HEPES (1 M, pH 7.3) was purchased from Amresco (Solon, OH, USA) and used as a buffer solution after dilution with ultrapure water. DTT (molecular biology grade DNase and RNase free), sodium dextran sulfate (Mw = 5000 Da), and phosphate buffered saline (PBS) were purchased from Wako Pure Chemical Industries Ltd. (Osaka, Japan). The luciferase-expressing human cervical cancer cell line, HeLa-Luc, was purchased from Caliper LifeScience (Hopkinton, MA, USA). Fetal bovine serum (FBS) was purchased from Dainippon Sumitomo Pharma Co., Ltd. (Osaka, Japan). Luciferin as a substrate for luciferase was purchased from Summit Pharmaceutical International (Tokyo, Japan). 10 × TBE running buffer was purchased from Invitrogen (Carlsbad, CA, USA). SYBR Green II and agarose were purchased from Takara Bio (Shiga, Japan). Luciferase Assay System Kit was purchased from Promega Co. (Madison, WI, USA). ExGen500 was purchased from Fermentas Life Sciences (Burlington, Canada). Dimethyl 3,3′-dithiobispropionimidate.HCl (DTBP) and slide-a-lyzer dialysis cassettes (MWCO = 3500 Da) were obtained from Thermo Scientific (Rockford, IL, USA).

2.2. Synthesis of PEG-PLL(MPA)

PEG-PLL bearing 1-(3-mercaptopropyl)amidine (MPA) groups in the lysine side chains (PEG-PLL(MPA)) was synthesized by the reaction of lysine primary amines with imidoesters of DTBP (Supporting Scheme 1), as previously described [28]. PEG-PLL (Mw of PEG = 12000; degree of polymerization (DP) of PLL = 88) (300 mg, 0.6 mmol amine) was dissolved in 200 mM sodium borate, pH 9.0 (60 mL) before adding DTBP (308 mg, 1.4 mmol, 1.5 equiv relative to lysine amines). The reaction was stirred at room temperature for 45 min, transferred to slide-a-lyzer dialysis cassettes, and then dialyzed against 10 mM phosphate buffer with 150 mM NaCl (pH 7.4) for 1.5 h to remove unreacted DTBP. After the recovery of the reaction mixture, DTT (300 mg) was added in order to generate thiol groups in the polymer side chains. The reaction was stirred at room temperature for 30 min before being transferred to slide-a-lyzer dialysis cassettes to perform dialysis against 10 mM phosphate buffer containing 150 mM NaCl (pH 6.0) for 2 h and distilled water for another 2 h with rapid stirring. The dialyzed polymer solution was passed through a 0.2 μm filter and lyophilized to obtain PEG-PLL(MPA) as a chloride salt form (299 mg, yield: 83%). The substitution degree of DTBP in the PLL side chain was determined to be 90% from the ^{1}H NMR spectrum based on the peak intensity ratio of the β, γ, and δ-methylene protons of Lys ($-(CH_2)_3-$, δ = 1.3–1.9 ppm) to the protons of mercaptoethyl groups ($HS-(CH_2)_2-$, δ = 2.7–2.9 ppm) (Supporting Fig. 1).

2.3. Preparation of PEGylated cross-linked polyplexes (PCPs) and their silica nanogelling

PCPs were prepared following the previously established protocol [28]. PEG-PLL(MPA) was dissolved in 10 mM HEPES buffer (pH 7.4) to produce a 5 mg/mL polymer stock solution having 12.9 mM of amidine groups. For complexation with siRNA (Mw = ~13000 Da), an aliquot of the stock solution was diluted with 10 mM HEPES buffer (pH 7.4) and then mixed with the same volume of 10 mM HEPES buffer (pH 7.4) containing 200 mM DTT. The polymer solution was incubated for 30 min at

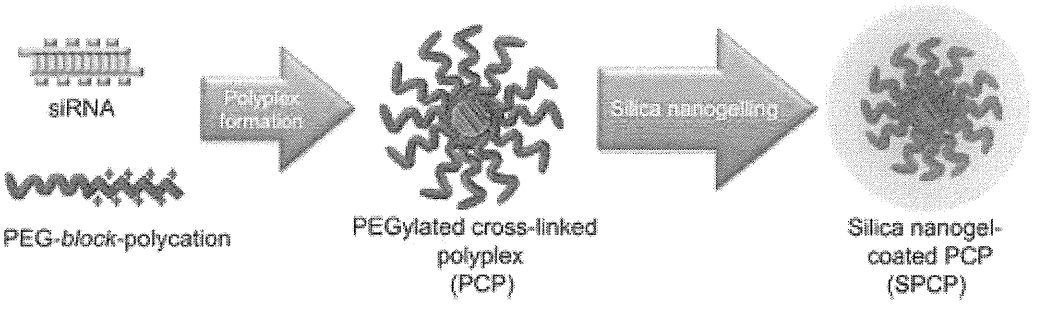

Fig. 1. Schematic illustration of preparation of PEGylated cross-linked polyplexes (PCPs) as a platform and their silica nanogelling for construction of silica nanogel-coated PCPs (SPCPs).